



HAL
open science

Unequal anthropogenic enrichment of mercury in Earth's Northern and Southern Hemispheres

Chuxian Li, Jeroen E Sonke, Gaël Le Roux, Natalia Piotrowska, Nathalie van Der Putten, Stephen J Roberts, Tim Daley, Emma Rice, Roland Gehrels, Maxime Enrico, et al.

► **To cite this version:**

Chuxian Li, Jeroen E Sonke, Gaël Le Roux, Natalia Piotrowska, Nathalie van Der Putten, et al.. Unequal anthropogenic enrichment of mercury in Earth's Northern and Southern Hemispheres. ACS Earth and Space Chemistry, In press, 10.1021/acsearthspacechem.0c00220 . hal-03007738

HAL Id: hal-03007738

<https://hal.science/hal-03007738v1>

Submitted on 16 Nov 2020

HAL is a multi-disciplinary open access archive for the deposit and dissemination of scientific research documents, whether they are published or not. The documents may come from teaching and research institutions in France or abroad, or from public or private research centers.

L'archive ouverte pluridisciplinaire **HAL**, est destinée au dépôt et à la diffusion de documents scientifiques de niveau recherche, publiés ou non, émanant des établissements d'enseignement et de recherche français ou étrangers, des laboratoires publics ou privés.

Unequal anthropogenic enrichment of mercury in Earth's Northern and Southern Hemispheres

Chuxian Li^{1,2}, Jeroen E. Sonke^{2§}, Gaël Le Roux¹, Natalia Piotrowska³, Nathalie Van der Putten⁴, Stephen J. Roberts⁵, Tim Daley⁶, Emma Rice⁶, Roland Gehrels⁷, Maxime Enrico^{1,2,8}, Dmitri Mauquoy⁹, Thomas P. Roland¹⁰, François De Vleeschouwer¹¹

1. Laboratoire écologie fonctionnelle et environnement, Université de Toulouse, CNRS, Toulouse, France

2. Laboratoire Géosciences Environnement Toulouse, Université de Toulouse, CNRS, IRD, UPS, Toulouse, France.

3. Silesian University of Technology, Institute of Physics-CSE, Gliwice, Poland.

4. Faculty of Science, Vrije Universiteit Amsterdam, the Netherlands.

5. British Antarctic Survey, Cambridge, UK

6. School of Geography, Earth and Environmental Sciences, Plymouth University, Plymouth PL4 8AA, UK

7. Department of Environment & Geography, University of York, Heslington, York YO10 5NG, UK

8. Harvard John A. Paulson School of Engineering & Applied Sciences, Harvard University, Cambridge, MA, USA

9. Geography and Environment, School of Geosciences, University of Aberdeen, St Mary's Building, Aberdeen, AB24 3UF, UK

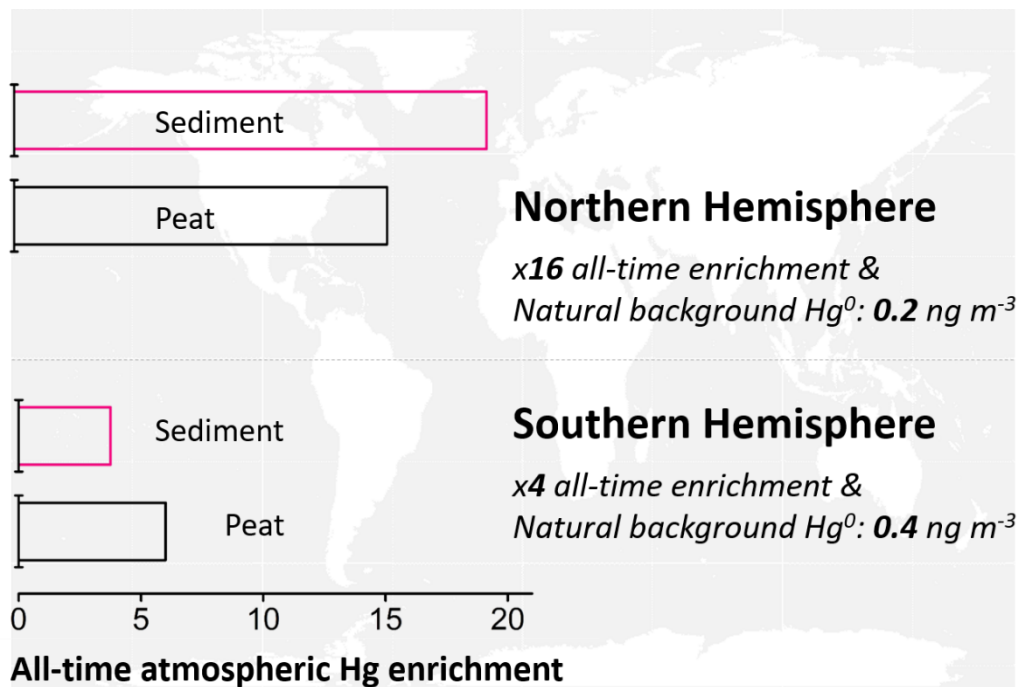
10. Geography, College of Life and Environmental Sciences, University of Exeter, UK

11. Instituto Franco-Argentino para el Estudio delClima y sus Impactos (UMI 3351 IFAECI/CNRS-CONICET-UBA), Universidad de Buenos Aires, Argentina

[§] Corresponding author: jeroen.sonke@get.omp.eu

Keywords: mercury, enrichment, peat, sediment, archive, hemisphere, deposition

TOC Figure



Abstract: Remote Northern (NH) and Southern Hemisphere (SH) lake sediment and peat records of mercury (Hg) deposition show a $\times 3$ to $\times 5$ Hg enrichment since pre-industrial times ($<1880\text{AD}$), leading to the perception that global atmospheric Hg enrichment is moderate and uniform across the hemispheres. Anthropogenic Hg emissions in the NH are, however, approximately four times higher than in the SH. Here we reconstruct atmospheric Hg deposition in four remote SH peatlands and review sediment and peat Hg records from both hemispheres. We observe a $\times 4$ all-time enrichment in SH Hg deposition from pre-anthropogenic ($<1450\text{AD}$) to late 20th century periods, which is lower than the large $\times 16$ all-time enrichment in NH Hg deposition. We attribute this difference to lower anthropogenic Hg emissions in the SH, and higher natural atmospheric SH Hg concentrations, supported by $\times 2$ higher natural background Hg accumulation in SH peat records. We suggest that the higher SH natural atmospheric Hg deposition reflects the SH land-ocean distribution, and is driven by important SH marine Hg emissions. Our findings indicate that atmospheric Hg background levels and anthropogenic enrichment in both hemispheres are different and should be taken into account in international Hg assessments and environmental policy.

Introduction:

Mercury (Hg) is a toxic trace metal that affects wildlife and human health ¹⁻⁴. Hg is discharged into the environment by natural processes, such as volcanism, chemical and physical weathering, and by human activities, including mining, coal burning and intentional use ⁵⁻⁷. Elemental Hg⁰, the dominant form of emissions, has a long atmospheric residence time of 6 to 12 months, which allows for its intra-hemispheric dispersion before being deposited to the Earth's surface, including remote environments ⁸. Assessments of the extent of global Hg pollution have relied upon natural archives of Hg accumulation (e.g. sediment ^{9,10}, peat ¹¹, ice cores ¹²), and on estimates of natural and anthropogenic Hg emissions ⁷.

Since early work on lake sediment cores in the 1970s ¹³, hundreds of remote ²¹⁰Pb dated sediment cores have documented an approximate three- to five-fold increase in Hg accumulation rates (HgAR) from pre-industrial (1760-1880 AD) times to the late 20th century ¹⁴⁻¹⁹. A comprehensive review in 2007 concluded that sediment records were more reliable than peat records in recording atmospheric HgAR ¹⁷. Inferred higher Hg accumulation in peat records was thought to be related to ²¹⁰Pb mobility, and peat mass loss during remineralization. A recent review study ¹⁸ indicated that earlier peat vs sediment comparisons ¹⁷ used different reference periods to calculate Hg enrichment. Using coherent reference periods, dozens of peat archives and a small number of glacier ice cores also document 3 to 5-fold enrichment factors, similar to sediment records, since pre-industrial times (EF_{preind}) ^{14,18}. Both sediment and peat records have strengths and weaknesses, with ²¹⁰Pb and Hg mobility during sediment diagenesis and peat decomposition being potential factors of bias ²⁰⁻²². Yet, both archives at remote locations record broadly similar Hg accumulation profiles across the past millennium, despite differences in archive functioning, and therefore warrant further comparison across Earth's two hemispheres. Regarding archive functioning, lake sediments integrate Hg deposition across a larger watershed, transient Hg storage in soils, followed by Hg run-off and in-lake cycling, leading to a longer Hg residence-time before deposition into sediments. Peatlands integrate Hg deposition directly from the atmosphere ^{18,23,24}, leading to a more direct response of peat archives to atmospheric Hg⁰ concentrations. This can generally be recognized by the 2-fold drop in HgAR from the 1970s to the 1990s in peat ¹⁸, which is absent in sediment records, and which mirrors the well-documented decrease in Hg emissions and observed atmospheric Hg⁰ concentrations ^{7,25,26}. A comparison of Hg stable isotope composition of peat and lake sediments indicates that in both archives 75% of Hg derives from uptake of atmospheric Hg⁰ ²³, which further justifies comparing both archives.

Longer radiocarbon-dated NH sediment and peat cores record changes in the natural background Hg accumulation during pre-colonial times (pre-1450AD), before large-scale mining practices, and

indicate a more dramatic difference in Hg deposition. Millennial sediment and peat records show that HgAR already increased five-fold during the earlier transition from pre-large-scale mining to pre-colonial times around approximately 1450 AD¹⁸. As a consequence, all-time anthropogenic Hg enrichment factors (EF_{alltime} , the ratio of 20th century to pre-1450 AD HgAR) determined from sediment and peat records range from 16 to 26¹⁸. The cause for the increase in NH Hg enrichment around 1450 AD has been debated. Some Hg inventory and modeling studies have argued for enhanced Hg emissions from Spanish colonial silver and gold mining²⁷⁻²⁹. Other studies argue that Hg associated with mining has been immobilized in mining waste, rather than volatilized^{1,9,30}. A study on Hg stable isotopes in peat has recently shown evidence how enhanced deforestation during the Middle Ages may have impacted regional atmospheric Hg dynamics in Europe with lower vegetation uptake of Hg, and wood burning emissions leading to enhanced atmospheric Hg concentrations and deposition²⁵. What nearly all the above cited studies have in common is that they are situated in the northern hemisphere (NH) where the majority of historical anthropogenic Hg emissions and studies have taken place. Relative to the NH, anthropogenic Hg emissions in the SH have continuously been four times lower³¹. Reviews of anthropogenic Hg enrichment in the environment generally provide a global picture without differentiating between the hemispheres^{20,32-34}. Lake sediment records of Hg accumulation have been studied in the SH and are reviewed here. Three southern hemisphere (SH) peat records have been studied for HgAR^{35,36}, but are all incomplete (see Methods, and Extended Data 2) and preclude a rigorous assessment of SH atmospheric Hg enrichment based on both sediment and peat archives.

The aim of this study is therefore to investigate potential differences in anthropogenic Hg enrichment in Earth's SH and NH. We hypothesize that, in regard of the lower historical SH anthropogenic Hg emissions, enrichment will also be lower. We extend the limited number of peat archives studied in the SH by investigating Hg accumulation rates in four new radiocarbon and ²¹⁰Pb and ¹⁴C bomb-pulse dated SH peat records. We then review all the existing SH sediment and peat HgAR (Extended Data 2), compare Hg enrichments factors to the NH, and discuss findings in the context of revised volcanic Hg emissions, published historical anthropogenic Hg emissions, and Hg cycling in both hemispheres. We do not include glacier ice cores in our review due to the limited number of studies available. Four reference time periods, operationally defined for NH natural archives elsewhere^{18,19}, will be used throughout: natural background (pre-1450AD), pre-industrial period (1450-1880 AD), 20th century extended HgAR maximum (20Cmax, approximately from 1940-1990; see also Methods), and the recent post-1990 modern period.

Materials & Methods

The study sites. We investigate four new cores from remote ombrotrophic peat lands in the SH mid-latitudes: Amsterdam Island (AMS, S-Indian Ocean), Falkland Islands (SCB, San Carlos bog, Islas Malvinas, S-Atlantic Ocean), Andorra and Harberton (AND, HBT, Tierra del Fuego, Argentina) (SI Appendix Table S1; Figure S1; Text S1; Extended Data 1). These four sites are situated in the southern westerly wind belt, far away from anthropogenic Hg sources, which makes them ideal recorders of SH remote atmospheric Hg deposition trends. Details about the field campaigns and sampling sites are given in SI Appendix Table S1 and Text S1. After collection, all the cores were photographed, described and packed in plastic film and PVC tubes and shipped to EcoLab, Toulouse, France. There, the cores were cut and processed following published trace metal clean protocols, freeze-dried and stored dry until analysis^{37,38}.

Chronology. Age model output of the AMS peat core is adopted from ref³⁹. In brief, a total of 20 samples were picked for plant macrofossils and subsequently radiocarbon-dated at the LMC14 Artemis Laboratory (Saclay, France, SacA code) or GADAM center (Gliwice, Poland, GdA code). Recent age control in the AMS peat core is based upon 4 post-bomb radiocarbon dates⁴⁰ together with ²¹⁰Pb dating using the constant rate of supply model, and ¹³⁷Cs, ²⁴¹Am⁴¹. A total of 9 samples of plant macrofossils/charcoal from SCB, 10 *Sphagnum* macrofossils from AND and 13 *Sphagnum* macrofossils from HBT were radiocarbon dated. These radiocarbon samples were pre-treated and graphitized at the GADAM center (Gliwice, Poland, GdA code)⁴². Subsequently, their ¹⁴C concentration in graphite was measured at the DirectAMS Laboratory (Bothell, WA, USA;⁴³). The NIST Oxalic Acid II standard was used for normalization, and black coal used as a blank. A total of 22 samples from the top 62 cm of the SCB peat core were selected for ²¹⁰Pb measurement by alpha counting to constrain the recent age (see Extended Data 1). The recent age control of the AND and HBT peat cores derive from 5 and 10 post-bomb radiocarbon dates, respectively^{40,44}.

Details of radiocarbon dates are summarized in SI Appendix Table S2. Age-depth models were generated from a combination of radiocarbon dating, post-bomb and ²¹⁰Pb dating with the Bacon package within R software⁴⁵, using the SHCal13 calibration curve for positive ¹⁴C ages⁴⁶, while the post-bomb radiocarbon dates were calibrated with SH zone 1-2 curve⁴⁷. The prior settings and model outputs are presented in SI Appendix Figure S2. The modelled median age was used for calculating and plotting HgAR against time (Figure 1). The average age uncertainties (1-sigma) derived from the age-depth models range from 1-5 years for the topmost part of the cores, up to ca. 100 years around 1000 AD. The

investigated peat profiles of AMS, SCB, AND, and HBT cover periods of 6600, 2000, 200 and 800 years, respectively. Corresponding mean peat accumulation rates are 0.76, 0.85, 3.6 and 0.91 mm yr⁻¹.

Peat Hg accumulation rates (HgAR). HgAR were calculated as the product of Hg concentration (ng g⁻¹), peat density (g cm⁻³) and peat mass accumulation rate (g m⁻² yr⁻¹). Peat density was determined for each 1 cm slice by measuring its volume using a Vernier caliper and dry peat mass after freeze-drying. Peat samples were analyzed for total Hg (THg) concentration on a combustion cold vapor atomic absorption spectrometer (CV-AAS, Milestone DMA-80) at the University of Toulouse, France. The IPE 176 CRM (Reed / *Phragmites communis*), NIST 1632d (Coal), and BCR 482 (Lichen) were analyzed with mean recoveries ranging from 93-100% (SI Appendix Table S3). Replicate/triplicate analyses of THg in peat samples were found to vary by less than 6% (1 σ). Profiles of peat Hg concentration in AMS, SCB, AND, and HBT are shown in SI Appendix Figure S5. Peat mass accumulation rate was determined from the age models and dry peat mass. All raw data are summarized in Extended Data 1.

Literature review, reference time periods and statistics. We expand on a previous literature review of sediment and peat Hg archives¹⁸. We examined the remote HgAR records from SH lake sediments and peat records in southern South America, lake sediments in New Zealand, lake sediments in East Africa, and lake sediments in Antarctica (see Extended data 2 for details). We exclude from our analysis: a lake sediment core 6 km downstream from the Potosi mine (Bolivia) with pronounced local mining influences on HgAR⁴⁹; a lake sediment core in the Patagonian volcanic zone with multiple tephra layers associated with high HgAR⁵⁰. Two remote Bolivian cores and one Peruvian core also showed evidence for the release of Hg due to regional Spanish colonial mining activities^{36,51}, but were retained in Extended Data 2. Extended Data 2 indicates which records were only partially used, often due to lack of recent ²¹⁰Pb or ¹⁴C bomb pulse dates. This applies in particular to three SH peat records, where one lacks a recent ²¹⁰Pb and recent ¹⁴C chronology and therefore 20Cmax and pre-industrial HgAR³⁶, one lacks pre-1988 layers⁴⁸, and one is nearly complete³⁵, except for the 1826-1935 period, which we extrapolate (see Extended Data 2).

We use four reference time periods, based on previous studies and originally derived for NH natural archives¹⁸: natural background (pre-1450AD), pre-industrial period (1450-1880AD), 20th century extended HgAR maximum (20Cmax, approx. 1940-1990), and the recent, modern period (post-1990AD). For each published study, we calculate mean HgAR during the four reference intervals. The operational cut-off years, e.g. 1450, 1880, 1990, represent the timing of changes in HgAR observed in NH sediment (n=49) and peat cores (n=19) reviewed here. Note that each archive and each regional context shows variation in the exact timing of gradual or abrupt increases (~1450, ~1880) or decreases (~1990) in HgAR

(Extended Data 2). Several long SH sediment records include the effect of climate change on variations in HgAR during the Holocene and since the last glacial maximum. Depending on watershed type and location these studies document substantial natural variability in HgAR that is beyond the scope of this study, but no less important. Therefore, in order to assess to the best of our ability the impact of humans on recent millennial atmospheric Hg enrichment, we integrated natural background HgAR between on average -1700BC to 1450AD, but on occasion as far back as 10,000BC (Extended Data 2). We define enrichment factors (EF) based on the evolution of mean HgAR during the four reference periods as follows:

$$EF_{\text{preind}} = \text{HgAR (20Cmax)} / \text{HgAR (pre-industrial)}$$

$$EF_{\text{alltime}} = \text{HgAR (20Cmax)} / \text{HgAR (natural background)}$$

$$EF_{\text{p/b}} = \text{HgAR (pre-industrial)} / \text{HgAR (natural background)}$$

$EF_{\text{mod/bck}} = \text{HgAR (modern)} / \text{HgAR (natural background)}$ Statistical descriptions are parametric (mean, standard deviation (SD)) for normally distributed HgAR and EF, and non-parametric (median, Q25% and Q75% quartiles, interquartile range (IQR)) for non-normally distributed HgAR and EF. Outlier tests were performed only on EFs, and observations were excluded (in *italics* in Extended Data 2) when they exceeded $2 \cdot \text{SD}$ around the mean, or $1.5 \cdot \text{IQR}$ around Q25% and Q75%. All data generated or analyzed during this study are included in the SI Appendix.

Results & Discussion

New southern hemisphere peat records

HgAR profiles in the four SH peat records show maximum values during the 20th century (Figure 1). Natural background (pre-1450 AD) HgAR in the HBT, SCB and AMS cores show a mean of $4.9 \pm 3.5 \mu\text{g m}^{-2} \text{yr}^{-1}$ (mean, 1σ , $n=33$ in 3 cores, Figure 1). Pre-industrial HgAR in the four cores averages $5.9 \pm 2.5 \mu\text{g m}^{-2} \text{yr}^{-1}$, 20Cmax HgAR is $20 \pm 7.9 \mu\text{g m}^{-2} \text{yr}^{-1}$, and modern HgAR is $9.7 \pm 2.9 \mu\text{g m}^{-2} \text{yr}^{-1}$ (means, 1σ , $n=4$, Figure 1). AND and HBT have more pronounced 20Cmax peaks than SCB and AMS, which is due to a combination of peaks in Hg concentration (Figure S5) and enhanced peat mass accumulation rate occurring simultaneously (Extended Data 1). Whereas absolute HgAR for the different time periods vary between cores, the relative HgAR changes between cores are similar and can be expressed by enrichment factors (EFs). The four SH cores show evidence for 3.1-fold (mean, $1\sigma=1.6$) enhanced net Hg deposition during the 20Cmax, compared to the pre-industrial period (EF_{preind} , Table 1), which at first sight appears similar to NH natural archives. SH historical HgARs have thus far been studied in 20 lake

sediment and 3 peat cores (see Methods and Extended Data 2 for full list). Figure 2 summarizes HgAR and EFs in all published SH sediment and peat records, as well as updated NH data for the reference periods of interest (Extended Data 2). The temporal evolution of HgAR in peat and sediment cores is similar between the NH and SH in a broad sense (Figure 2a, b). HgAR increases stepwise from natural background to pre-industrial and then to 20Cmax periods in both sediment and peat archives. Similar to NH peat records¹⁸, modern-day (post-1990) HgAR in SH peat decreases by a factor of 2 from 20Cmax values (SI Appendix Figure S4), in line with declining global anthropogenic Hg emissions and deposition from the 1970s to 2000s (Figure S6^{25,26}). Sediment records in both the NH and SH do not record this decrease (Figure S4), presumably due to the longer residence of Hg in lake catchment soils, leading to a slower recovery of Hg concentrations in soil run-off into lakes¹⁸.

Hemispheric trends in historical Hg enrichment

The historical evolution of trends in hemispheric HgARs is shown in EF_{preind} and EF_{alltime} diagrams (Figure 2c, 2d). Pre-industrial to 20Cmax enrichment in HgAR (EF_{preind}) is higher in peat compared to sediment in both NH and SH (Kruskal-Wallis test, NH, $P=0.01$; SH, $P=0.10$). EF_{preind} is higher in the NH than in the SH for sediment (3.1 vs 1.8), but not peat (4.6 vs 3.1; Kruskal-Wallis test, peat, $P=0.15$; sediment $P=0.001$; Figure 2c, 2d; Figure 3a). We find in particular that in long millennial NH records, HgAR increased 3.9-fold in peat and 3.7-fold in sediments across the natural background to pre-industrial periods around 1450AD ($EF_{\text{p/b}}$, Figure 2c, d, Table 2). In contrast, $EF_{\text{p/b}}$ in SH millennial records show negligible, mean 1.2-fold enrichment in peat, to a small, median 1.4-fold enrichment in sediments across the natural background (<1450AD) to pre-industrial periods. Consequently, all-time NH enrichment factors (EF_{alltime}), reach 16 in peat and 13 in sediments and are larger than the 6.0-fold and 3.8-fold Hg all-time enrichment in SH peat and sediments (Table 2; Figure 3B; Kruskal-Wallis test, $P = 0.02$ for peat, $P = 0.09$ for sediment). Historical Hg emission inventory and associated box modeling studies have suggested that the 4-fold increase in NH HgAR around 1450AD is related to Spanish colonial Hg and silver mining^{7,27}. This interpretation has been questioned by studies arguing that the associated emissions are overestimated^{1,9,52}. SH archives show little evidence of Spanish colonial mining impacts in South-America on large scale SH atmospheric Hg deposition (Figure 2). Similarly, neither NH peat, nor sediment records show evidence of a pronounced late 19th century peak in HgAR, in contrast to large estimated North American gold-rush Hg emissions⁷. Across the natural background and pre-industrial reference periods, the world's global population increased 5-fold from 0.22 to 1.2 billion⁵³. We therefore suggest that the 4-fold NH increase

in HgAR around 1450AD is more likely related to demography driven changes in land use and associated Hg emissions and deposition (e.g. deforestation²⁵, wood and peat combustion, urbanization), than to direct Spanish colonial mining emissions of Hg to the global pool. More research is needed to explore this in detail. In summary, our findings, based on combined sediment and peat archive HgAR observations, suggest that all-time atmospheric Hg enrichment during the 20Cmax period (1940-1990) reached 11-fold globally ($EF_{alltime} = 4-24$, 25%-75% quartiles, $n=39$), 16-fold in the NH ($EF_{alltime} = 10-30$, 25%-75% quartiles, $n=26$), and 4-fold in the SH ($EF_{alltime} = 2-6$, 25%-75% quartiles, $n=13$). Atmospheric Hg concentrations decreased from the 1970s to the 2000s by a factor of about 2, a trend that is recorded in the peat archive HgAR (Figure S4, S6). Natural background to modern period (1990-2010) Hg enrichment, $EF_{mod/bck}$, based on peat archives, is currently 10-fold globally (± 7.7 , 1σ , $n=18$), 12 in the NH (± 7.5 , 1σ , $n=14$) and 3 in the SH (± 2.5 , 1σ , $n=4$).

Natural and anthropogenic hemispheric Hg emissions

In the following sections we will further discuss this sizeable difference in hemispheric $EF_{alltime}$ in terms of NH and SH Hg emissions, and in terms of natural background HgAR. The all-time NH and SH enrichment factors, based on Hg deposition to natural archives, can be directly compared to independent estimates of NH and SH emission factors, i.e. $EF_{emission}$, the ratio of primary, i.e. first time, total Hg emission flux to natural Hg emission flux ($EF_{emission} = F_{anthro} + F_{natural} / F_{natural}$; Table 3). Streets et al. estimated global anthropogenic Hg emissions to the atmosphere of $2.4 \pm 0.5 \text{ Gg yr}^{-1}$ during the 20Cmax period (1940-1990)⁷. Natural Hg emissions are the sum of volcanic degassing and crustal degassing from naturally enriched soils. Passive, non-eruptive, volcanic degassing is an important direct natural source of Hg to the atmosphere, with a previously estimated total flux of $76 \pm 30 \text{ Mg yr}^{-1}$ (1σ) based on observed Hg/SO₂ ratios of $7.8 \pm 1.5 \times 10^{-6}$ and a global passive degassing SO₂ flux of 9.7 Tg yr^{-1} ^{54,55}. Recent advances in remote sensing of SO₂ from 2005-2015 indicate a higher SO₂ flux of $23.0 \pm 2.3 \text{ Tg yr}^{-1}$ (1σ)⁵⁶, which we use here to revise the global passive volcanic degassing Hg flux to $179 \pm 39 \text{ Mg yr}^{-1}$ (1σ). Eruptive volcanic SO₂ emissions are indicated to be one order of magnitude smaller than passive degassing at $2.6 \pm 2.6 \text{ Tg yr}^{-1}$ ⁵⁶. Assuming similar Hg/SO₂ ratios, we estimate eruptive volcanic Hg emissions at $20 \pm 20 \text{ Mg yr}^{-1}$, and total volcanic Hg emissions as the sum of eruptive and passive emissions at $200 \pm 60 \text{ Mg yr}^{-1}$ (1σ). Global emissions from naturally enriched soils can be estimated from reviews of flux chamber and soil Hg studies^{57,58} and equal $135 \pm 40 \text{ Mg yr}^{-1}$ (1σ , Table 3). These estimates indicate that global anthropogenic 20Cmax Hg emissions of 2.4 Gg yr^{-1} have been 7.3 times larger than

global natural Hg emissions of 0.34 Gg yr^{-1} , and result in a global EF_{emission} of 8.2. Volcanic SO_2 emissions are similar for the NH and SH (11.8 vs. 11.2 Tg yr^{-1})⁵⁶, leading to NH and SH Hg emission budgets of 0.1 Gg yr^{-1} each. We scale naturally enriched soil emissions with continental surface area, to estimate 91 and 44 Mg yr^{-1} in NH and SH. The 20Cmax 2.4 Gg yr^{-1} global anthropogenic Hg emissions to the atmosphere were released for 80% to the NH and 20% to the SH⁷. We therefore estimate hemispheric EF_{emission} for the NH at 11.2 ± 4.6 and for the SH at 4.4 ± 1.5 (1σ). The SH EF_{emission} of 4.4 is in good agreement with the natural archive-based SH EF_{alltime} of 4. The NH EF_{emission} of 11 however, underestimates the NH EF_{alltime} of 16 by 43%, suggesting that either the $2.0 \pm 0.5 \text{ Gg yr}^{-1}$ NH anthropogenic Hg emissions to air⁷ are underestimated, or that the NH natural primary emissions of $91 \pm 27 \text{ Mg yr}^{-1}$ are overestimated, or that inter-hemispheric exchange has transported NH anthropogenic Hg to the SH. There is a final caveat in this analysis that deserves a mention. We assume that the ill-constrained, but potentially important, submarine volcanic Hg flux⁵⁹ is locally or regionally deposited to marine sediments before any of it can be emitted to the atmosphere. This assumption is based on evidence for Hg scavenging in submarine hydrothermal plumes^{60,61}.

The most recent, 2018 UNEP global Hg assessment, which provides the state of the science basis for the implementation of the UNEP Minamata Convention on mercury, states that “Human activities have increased total atmospheric Hg concentrations by about 450% (i.e. a factor 4.5) above natural levels.”¹⁴. Our findings therefore suggest that modern (1990-2010) atmospheric Hg enrichment is larger, 10-fold globally. In addition we find consistently lower anthropogenic Hg enrichment in emissions and in deposition in the SH compared to the NH.

Hemispheric differences in Hg deposition and cycling

The important difference in NH and SH EF_{alltime} is not only related to hemispheric differences in primary Hg emissions, but also to differences in natural background atmospheric Hg concentrations and HgAR. A notable outcome of the new SH peat records is that the natural SH background HgAR of $4.3 \mu\text{g m}^{-2} \text{ yr}^{-1}$ in the SH mid-latitudes ($30\text{-}60^\circ\text{S}$) is $\times 2.5$ higher than the NH background HgAR of $1.7 \mu\text{g m}^{-2} \text{ yr}^{-1}$ in the NH mid-latitudes (Kruskal-Wallis test, $P=0.02$, Figures 2a, 3c, S3). Recent Hg stable isotope work on Hg deposition to vegetation and soils suggests that 75% derives from direct uptake of atmospheric Hg(0), and less from Hg(II) wet deposition^{23,25,62,63}. Consequently, peat vegetation Hg(0) uptake is primarily driven by atmospheric Hg(0) concentration and primary productivity²⁵. Peat vegetation primary productivity depends on climate, which, at the NH and SH mid-latitude sites we study and review, shows

similar mean annual air temperatures (NH, 6.7; SH, 6.3 °C), precipitation (NH, 1110; SH, 1120 mm y⁻¹) and cloud cover (NH, 72; SH 77%)⁶⁴. We therefore suggest that the marked NH/SH mid-latitude difference in HgAR is driven by ×2.5 higher natural atmospheric Hg concentrations in the SH, rather than climate factors. Climate factors, such as temperature and length of growth season only become visible in NH high latitude (>60°N), where HgAR are limited by peat bog primary productivity via the vegetation Hg⁰ pump²⁴. The observation that the SH natural background HgAR is ×2.5 higher than the NH background is likely an additional reason why the NH EF_{alltime} of 16 is much larger than the SH EF_{alltime} of 4.

Inter-hemispheric trends in atmospheric Hg have been previously investigated^{65,66}. Observed mean atmospheric Hg⁰ concentrations across monitoring networks for the modern, 1990-2010 period were 1.8 ng m⁻³ in the NH and 1.2 ng m⁻³ in the SH^{67,68}. Modern-day SH Hg⁰ concentrations are therefore higher than what would be expected based on estimates of modern NH and SH primary Hg emissions of 1.6 and 0.7 Gg yr⁻¹ (Table 3). Inter-hemispheric transport of NH Hg⁰ to the SH potentially contributes to the high SH Hg⁰ concentrations. A key difference between the NH and SH is the land-ocean distribution, with the SH being only 19% land covered and the NH 39%. The land-ocean distribution plays an important role in atmospheric boundary layer Hg dynamics. A study on atmospheric Hg⁰ seasonality, which is more pronounced in the NH and quasi-absent in the SH, suggested that the vegetation Hg pump, i.e. the foliar uptake of Hg⁰ and sequestration in soils, is an important driver of NH atmospheric Hg⁰ seasonality²⁴. The SH has a smaller terrestrial vegetation and soil pool, and we speculate that the SH has relatively higher atmospheric Hg⁰ due to a weaker vegetation Hg pump. In addition coupled ocean-atmosphere Hg chemistry and transport models find stronger marine Hg⁰ evasion in the SH than in the NH, mainly due to upwelling of Hg rich deep waters in the Southern Ocean^{19,69}. The model studies suggest that SH atmospheric Hg⁰ is largely controlled by these SH marine Hg⁰ emissions^{8,19}. These findings were recently confirmed by long-term observations on Hg⁰ seasonality at the Cape Point monitoring station in South Africa⁷⁰. The 2-fold higher SH natural background HgAR in peat therefore echoes the higher than expected modern SH atmospheric Hg⁰ concentrations, and both can potentially be explained by the hemispheric land-ocean distribution.

We use peat EF_{mod/bck} for both hemispheres (Table 2) to estimate what natural atmospheric Hg⁰ concentrations may have been during pre-1450AD times. Dividing modern-day mean NH and SH atmospheric Hg⁰ concentrations of 1.8 and 1.2 ng m⁻³ by EF_{mod/bck} yields natural background atmospheric Hg concentrations of 0.2 and 0.4 ng m⁻³ for the NH and SH. In summary, the lower SH enrichment in atmospheric Hg appears to be caused by a combination of lower SH anthropogenic Hg emissions, and

higher SH background Hg concentrations. We speculate that the higher SH atmospheric background is driven by a lower SH land/ocean ratio which limits the terrestrial vegetation Hg pump and sustains higher natural marine Hg emissions. Overall, our findings suggest that both background Hg concentrations and all-time Hg enrichment in the NH and SH are different and should be taken into account in environmental policy objectives.

Acknowledgements

Field work was funded by the French Polar Institute (IPEV, Brest, France) through the IPEV Programmes 1066 “PARAD” (to F.D.V.) and 1065 PALATIO (to N.V.P. and E. Michel). J.E.S. acknowledges funding from the H2020 ERA-PLANET (689443) iGOSP and iCUPE programmes. We thank the South Atlantic Environmental Research Institute (SAERI) for providing laboratory facilities in the Falkland Islands and E. Brook (Falkland Islands Government Training Centre) for logistical support. We are grateful to N. Marchand (IPEV) for the logistical support, C. Marteau for making the sampling possible in very restricted areas of the TAAF Nature Reserve, and N. Roberts for help processing the San Carlos core and scientific discussions. We thank A. Coronato, R. López and V. Pancotto from CADIC-CONICET (Ushuaia) for the field campaigns in Andorra and Harberton. Radiocarbon ages were obtained as part of the IDEX Peat3 project of the University of Toulouse and through the national service support: Artemis-INSU-CNRS (to G.L.R.). C.L.’s PhD is supported by a scholarship from the China Scholarship Council. We thank 12 anonymous reviewers for their constructive comments on the various versions of this paper, and editor JD Blum for handling the final version.

Author Contributions

J.E.S and F.D.V initiated and designed the project. All authors were involved in field sampling, laboratory analyses, and/or data analysis. C.L. and J.E.S wrote the manuscript on which all authors commented.

Data availability statement

All data generated or analyzed during this study are included in this published article (and its SI Appendix).

References

- (1) Outridge, P. M.; Mason, R. P.; Wang, F.; Guerrero, S.; Heimbürger-Boavida, L. E. Updated Global and Oceanic Mercury Budgets for the United Nations Global Mercury Assessment 2018. *Environ. Sci. Technol.* **2018**, *52* (20), 11466–11477. <https://doi.org/10.1021/acs.est.8b01246>.
- (2) Mason, R. P.; Choi, A. L.; Fitzgerald, W. F.; Hammerschmidt, C. R.; Lamborg, C. H.; Soerensen, A. L.; Sunderland, E. M. Mercury Biogeochemical Cycling in the Ocean and Policy Implications. *Environ. Res.* **2012**, *119*, 101–117. <https://doi.org/10.1016/j.envres.2012.03.013>.

- (3) Chen, C.; Amirbahman, A.; Fisher, N.; Harding, G.; Lamborg, C.; Nacci, D.; Taylor, D. Methylmercury in Marine Ecosystems: Spatial Patterns and Processes of Production, Bioaccumulation, and Biomagnification. *Ecohealth* **2008**, *5* (4), 399–408. <https://doi.org/10.1007/s10393-008-0201-1>.
- (4) Sunderland, E. M. Mercury Exposure from Domestic and Imported Estuarine and Marine Fish in the U.S. Seafood Market. *Environ. Health Perspect.* **2007**, *115* (235–242).
- (5) Pirrone, N.; Cinnirella, S.; Feng, X.; Finkelman, R. B.; Friedli, H. R.; Leaner, J.; Mason, R.; Mukherjee, A. B.; Stracher, G. B.; Streets, D. G.; Telmer, K. Global Mercury Emissions to the Atmosphere from Anthropogenic and Natural Sources. *Atmospheric Chem. Phys.* **2010**, *10* (13), 5951–5964. <https://doi.org/10.5194/acp-10-5951-2010>.
- (6) Pacyna, E. G.; Pacyna, J. M.; Sundseth, K.; Munthe, J.; Kindbom, K.; Wilson, S.; Steenhuisen, F.; Maxson, P. Global Emission of Mercury to the Atmosphere from Anthropogenic Sources in 2005 and Projections to 2020. *Atmos. Environ.* **2010**, *44* (20), 2487–2499. <https://doi.org/10.1016/j.atmosenv.2009.06.009>.
- (7) Streets, D. G.; Horowitz, H. M.; Jacob, D. J.; Lu, Z.; Levin, L.; ter Schure, A. F. H.; Sunderland, E. M. Total Mercury Released to the Environment by Human Activities. *Environ. Sci. Technol.* **2017**, *51* (11), 5969–5977. <https://doi.org/10.1021/acs.est.7b00451>.
- (8) Horowitz, H. M.; Jacob, D. J.; Zhang, Y.; Dibble, T. S.; Slemr, F.; Amos, H. M.; Schmidt, J. A.; Corbitt, E. S.; Marais, E. A.; Sunderland, E. M. A New Mechanism for Atmospheric Mercury Redox Chemistry: Implications for the Global Mercury Budget. *Atmospheric Chem. Phys.* **2017**, *17* (10), 6353–6371. <https://doi.org/10.5194/acp-17-6353-2017>.
- (9) Engstrom, D. R.; Fitzgerald, W. F.; Cooke, C. A.; Lamborg, C. H.; Drevnick, P. E.; Swain, E. B.; Balogh, S. J.; Balcom, P. H. Atmospheric Hg Emissions from Preindustrial Gold and Silver Extraction in the Americas: A Reevaluation from Lake-Sediment Archives. *Environ. Sci. Technol.* **2014**, *48* (12), 6533–6543. <https://doi.org/10.1021/es405558e>.
- (10) Fitzgerald, W. F.; Engstrom, D. R.; Mason, R. P.; Nater, E. A. The Case for Atmospheric Mercury Contamination in Remote Areas. *Environ. Sci. Technol.* **1998**, *32* (1), 1–7. <https://doi.org/10.1021/es970284w>.
- (11) Martınez-Cortizas, A. Mercury in a Spanish Peat Bog: Archive of Climate Change and Atmospheric Metal Deposition. *Science* **1999**, *284* (5416), 939–942. <https://doi.org/10.1126/science.284.5416.939>.
- (12) Schuster, P. F.; Krabbenhoft, D. P.; Naftz, D. L.; Cecil, L. D.; Olson, M. L.; Dewild, J. F.; Susong, D. D.; Green, J. R.; Abbott, M. L. Atmospheric Mercury Deposition during the Last 270 Years: A Glacial Ice Core Record of Natural and Anthropogenic Sources. *Environ. Sci. Technol.* **2002**, *36* (11), 2303–2310. <https://doi.org/10.1021/es0157503>.
- (13) Thomas, R. L. The Distribution of Mercury in the Sediments of Lake Ontario. *Can. J. Earth Sci.* **1972**, *9* (6), 636–651. <https://doi.org/10.1139/e72-054>.
- (14) UNEP. *Global Mercury Assessment 2018*; 2018.
- (15) Fitzgerald, W. F.; Engstrom, D. R.; Mason, R. P.; Nater, E. A. The Case for Atmospheric Mercury Contamination in Remote Areas. *Environ. Sci. Technol.* **1998**, *32* (1), 1–7. <https://doi.org/10.1021/es970284w>.
- (16) Engstrom, D. R.; Fitzgerald, W. F.; Cooke, C. A.; Lamborg, C. H.; Drevnick, P. E.; Swain, E. B.; Balogh, S. J.; Balcom, P. H. Atmospheric Hg Emissions from Preindustrial Gold and Silver Extraction in the Americas: A Reevaluation from Lake-Sediment Archives. *Environ. Sci. Technol.* **2014**, *48* (12), 6533–6543. <https://doi.org/10.1021/es405558e>.
- (17) Biester, H.; Bindler, R.; Martınez-Cortizas, A.; Engstrom, D. R. Modeling the Past Atmospheric Deposition of Mercury Using Natural Archives. *Environ. Sci. Technol.* **2007**, *41* (14), 4851–4860. <https://doi.org/10.1021/es0704232>.

- (18) Amos, H. M.; Sonke, J. E.; Obrist, D.; Robins, N.; Hagan, N.; Horowitz, H. M.; Mason, R. P.; Witt, M.; Hedgecock, I. M.; Corbitt, E. S.; Sunderland, E. M. Observational and Modeling Constraints on Global Anthropogenic Enrichment of Mercury. *Environ. Sci. Technol.* **2015**, *49* (7), 4036–4047. <https://doi.org/10.1021/es5058665>.
- (19) Zhang, Y.; Jaeglé, L.; Thompson, L.; Streets, D. G. Six Centuries of Changing Oceanic Mercury: Anthropogenic Mercury in Ocean. *Glob. Biogeochem. Cycles* **2014**, *28* (11), 1251–1261. <https://doi.org/10.1002/2014GB004939>.
- (20) Biester, H.; Bindler, R.; Martinez-Cortizas, A.; Engstrom, D. R. Modeling the Past Atmospheric Deposition of Mercury Using Natural Archives. *Environ. Sci. Technol.* **2007**, *41* (14), 4851–4860. <https://doi.org/10.1021/es0704232>.
- (21) Cooke, C. A.; Hobbs, W. O.; Michelutti, N.; Wolfe, A. P. Reliance on Pb-210 Chronology Can Compromise the Inference of Preindustrial Hg Flux to Lake Sediments. *Environ. Sci. Technol.* **2010**, *44* (6), 1998–2003. <https://doi.org/10.1021/es9027925>.
- (22) Abril, J. M.; Brunskill, G. Evidence That Excess 210Pb Flux Varies with Sediment Accumulation Rate and Implications for Dating Recent Sediments. *J. Paleolimnol.* **2014**, *52*. <https://doi.org/10.1007/s10933-014-9782-6>.
- (23) Enrico, M.; Roux, G. L.; Maruszczak, N.; Heimbürger, L.-E.; Claustres, A.; Fu, X.; Sun, R.; Sonke, J. E. Atmospheric Mercury Transfer to Peat Bogs Dominated by Gaseous Elemental Mercury Dry Deposition. *Environ. Sci. Technol.* **2016**, *50* (5), 2405–2412. <https://doi.org/10.1021/acs.est.5b06058>.
- (24) Jiskra, M.; Sonke, J. E.; Obrist, D.; Bieser, J.; Ebinghaus, R.; Myhre, C. L.; Pfaffhuber, K. A.; Wängberg, I.; Kyllönen, K.; Worthy, D.; Martin, L. G.; Labuschagne, C.; Mkololo, T.; Ramonet, M.; Magand, O.; Dommergue, A. A Vegetation Control on Seasonal Variations in Global Atmospheric Mercury Concentrations. *Nat. Geosci.* **2018**, *11* (4), 244–250. <https://doi.org/10.1038/s41561-018-0078-8>.
- (25) Enrico, M.; Le Roux, G.; Heimbürger, L.-E.; Van Beek, P.; Souhaut, M.; Chmeleff, J.; Sonke, J. E. Holocene Atmospheric Mercury Levels Reconstructed from Peat Bog Mercury Stable Isotopes. *Environ. Sci. Technol.* **2017**, *51* (11), 5899–5906. <https://doi.org/10.1021/acs.est.6b05804>.
- (26) European Monitoring and Evaluation Programme. <https://www.emep.int/> 2016.
- (27) Streets, D. G.; Devane, M. K.; Lu, Z.; Bond, T. C.; Sunderland, E. M.; Jacob, D. J. All-Time Releases of Mercury to the Atmosphere from Human Activities. *Environ. Sci. Technol.* **2011**, *45* (24), 10485–10491. <https://doi.org/10.1021/es202765m>.
- (28) Streets, D. G.; Horowitz, H. M.; Lu, Z.; Levin, L.; Thackray, C. P.; Sunderland, E. M. Five Hundred Years of Anthropogenic Mercury: Spatial and Temporal Release Profiles. *Environ. Res. Lett.* **2019**, *14* (8), 084004. <https://doi.org/10.1088/1748-9326/ab281f>.
- (29) Amos, H. M.; Jacob, D. J.; Streets, D. G.; Sunderland, E. M. Legacy Impacts of All-Time Anthropogenic Emissions on the Global Mercury Cycle: GLOBAL IMPACTS OF LEGACY MERCURY. *Glob. Biogeochem. Cycles* **2013**, *27* (2), 410–421. <https://doi.org/10.1002/gbc.20040>.
- (30) Cooke, C. A.; Hintelmann, H.; Ague, J. J.; Burger, R.; Biester, H.; Sachs, J. P.; Engstrom, D. R. Use and Legacy of Mercury in the Andes. *Environ. Sci. Technol.* **2013**, *47* (9), 4181–4188. <https://doi.org/10.1021/es3048027>.
- (31) Streets, D. G.; Horowitz, H. M.; Jacob, D.; Lu, Z.; Levin, L.; ter Schure, A. F. H.; Sunderland, E. M. Total Mercury Released to the Environment by Human Activities. *Environ. Sci. Technol.* **2017**, *51* (11), 5969–5977. <https://doi.org/10.1021/acs.est.7b00451>.
- (32) Amos, H. M.; Sonke, J. E.; Obrist, D.; Robins, N.; Hagan, N.; Horowitz, H. M.; Mason, R. P.; Witt, M.; Hedgecock, I. M.; Corbitt, E. S.; Sunderland, E. M. Observational and Modeling Constraints on Global Anthropogenic Enrichment of Mercury. *Environ. Sci. Technol.* **2015**, *49* (7), 4036–4047. <https://doi.org/10.1021/es5058665>.

- (33) Cooke, C. A.; Martínez-Cortizas, A.; Bindler, R.; Gustin, M. S. Environmental Archives of Atmospheric Hg Deposition – A Review. *Sci. Total Environ.* **2020**, *709*, 134800. <https://doi.org/https://doi.org/10.1016/j.scitotenv.2019.134800>.
- (34) Lindberg, S.; Bullock, R.; Ebinghaus, R.; Engstrom, D.; Feng, X.; Fitzgerald, W.; Pirrone, N.; Prestbo, E.; Seigneur, C. A Synthesis of Progress and Uncertainties in Attributing the Sources of Mercury Deposition. *Ambio* **2007**, *36*, 19–32.
- (35) Biester, H.; Kilian, R.; Franzen, C.; Woda, C.; Mangini, A.; Schöler, H. F. Elevated Mercury Accumulation in a Peat Bog of the Magellanic Moorlands, Chile (53°S) – an Anthropogenic Signal from the Southern Hemisphere. *Earth Planet. Sci. Lett.* **2002**, *201* (3–4), 609–620. [https://doi.org/10.1016/S0012-821X\(02\)00734-3](https://doi.org/10.1016/S0012-821X(02)00734-3).
- (36) Guédron, S.; Ledru, M.-P.; Escobar-Torrez, K.; Develle, A. L.; Brisset, E. Enhanced Mercury Deposition by Amazonian Orographic Precipitation: Evidence from High-Elevation Holocene Records of the Lake Titicaca Region (Bolivia). *Palaeogeogr. Palaeoclimatol. Palaeoecol.* **2018**, *511*, 577–587. <https://doi.org/10.1016/j.palaeo.2018.09.023>.
- (37) Le Roux, G.; Vleeschouwer, F. Preparation of Peat Samples for Inorganic Geochemistry Used as Palaeoenvironmental Proxies. *Mires Peat* **2011**, *7*.
- (38) Givélet, N.; Le Roux, G.; Cheburkin, A.; Chen, B.; Frank, J.; Goodsite, M.; Kempter, H.; Krachler, M.; Noernberg, T.; Rausch, N.; Rheinberger, S.; Roos-Barraclough, F.; Sapkota, A.; Scholz, C.; Shotyk, W. Suggested Protocol for Collecting, Handling and Preparing Peat Cores and Peat Samples for Physical, Chemical, Mineralogical and Isotopic Analyses. *J. Environ. Monit.* **2004**, *6* (5), 481–492. <https://doi.org/10.1039/b401601g>.
- (39) Li, C.; Sonke, J. E.; Le Roux, G.; Van der Putten, N.; Piotrowska, N.; Jeandel, C.; Mattielli, N.; Benoit, M.; Wiggs, G. F. S.; De Vleeschouwer, F. Holocene Dynamics of the Southern Westerly Winds over the Indian Ocean Inferred from a Peat Dust Deposition Record. *Quat. Sci. Rev.* **2020**, *231*, 106169. <https://doi.org/10.1016/j.quascirev.2020.106169>.
- (40) Goodsite, M. E.; Rom, W.; Heinemeier, J.; Lange, T.; Ooi, S.; Appleby, P. G.; Shotyk, W.; van der Knaap, W. O.; Lohse, C.; Hansen, T. S. High-Resolution AMS ¹⁴C Dating of Post-Bomb Peat Archives of Atmospheric Pollutants. *Radiocarbon* **2001**, *43* (2B), 495–515. <https://doi.org/10.1017/S0033822200041163>.
- (41) Appleby, P. G. Chronostratigraphic Techniques in Recent Sediments. In *Tracking Environmental Change Using Lake Sediments*; Last, W. M., Smol, J. P., Eds.; Kluwer Academic Publishers: Dordrecht, 2002; Vol. 1, pp 171–203. https://doi.org/10.1007/0-306-47669-X_9.
- (42) Piotrowska, N. Status Report of AMS Sample Preparation Laboratory at GADAM Centre, Gliwice, Poland. *Nucl. Instrum. Methods Phys. Res. Sect. B Beam Interact. Mater. At.* **2013**, *294*, 176–181. <https://doi.org/10.1016/j.nimb.2012.05.017>.
- (43) Zoppi, U.; Crye, J.; Song, Q.; Arjomand, A. Performance Evaluation of the New AMS System at Accium BioSciences. *Radiocarbon* **2007**, *49* (1), 171–180. <https://doi.org/10.1017/S0033822200041990>.
- (44) Davies, L. J.; Appleby, P.; Jensen, B. J. L.; Magnan, G.; Mullan-Boudreau, G.; Noernberg, T.; Shannon, B.; Shotyk, W.; van Bellen, S.; Zaccone, C.; Froese, D. G. High-Resolution Age Modelling of Peat Bogs from Northern Alberta, Canada, Using Pre- and Post-Bomb ¹⁴C, ²¹⁰Pb and Historical Cryptotephra. *Quat. Geochronol.* **2018**, *47*, 138–162. <https://doi.org/10.1016/j.quageo.2018.04.008>.
- (45) Blaauw, M.; Christen, J. A. Flexible Paleoclimate Age-Depth Models Using an Autoregressive Gamma Process. *Bayesian Anal.* **2011**, *6* (3), 457–474. <https://doi.org/10.1214/11-BA618>.
- (46) Hogg, A. G.; Hua, Q.; Blackwell, P. G.; Niu, M.; Buck, C. E.; Guilderson, T. P.; Heaton, T. J.; Palmer, J. G.; Reimer, P. J.; Reimer, R. W.; Turney, C. S. M.; Zimmerman, S. R. H. SHCal13 Southern

- Hemisphere Calibration, 0–50,000 Years Cal BP. *Radiocarbon* **2013**, *55* (4), 1889–1903. https://doi.org/10.2458/azu_js_rc.55.16783.
- (47) Hua, Q.; Barbetti, M.; Rakowski, A. Z. Atmospheric Radiocarbon for the Period 1950–2010. *Radiocarbon* **2013**, *55* (4), 2059–2072. https://doi.org/10.2458/azu_js_rc.v55i2.16177.
- (48) Lamborg, C. H.; Fitzgerald, W. F.; Damman, A. W. H.; Benoit, J. M.; Balcom, P. H.; Engstrom, D. R. Modern and Historic Atmospheric Mercury Fluxes in Both Hemispheres: Global and Regional Mercury Cycling Implications: MODERN AND HISTORIC FLUXES OF ATMOSPHERIC MERCURY. *Glob. Biogeochem. Cycles* **2002**, *16* (4), 51–1–51–11. <https://doi.org/10.1029/2001GB001847>.
- (49) Cooke, C. A.; Balcom, P. H.; Kerfoot, C.; Abbott, M. B.; Wolfe, A. P. Pre-Colombian Mercury Pollution Associated with the Smelting of Argentiferous Ores in the Bolivian Andes. *AMBIO* **2011**, *40* (1), 18–25. <https://doi.org/10.1007/s13280-010-0086-4>.
- (50) Ribeiro Guevara, S.; Meili, M.; Rizzo, A.; Daga, R.; Arribére, M. Sediment Records of Highly Variable Mercury Inputs to Mountain Lakes in Patagonia during the Past Millennium. *Atmospheric Chem. Phys.* **2010**, *10* (7), 3443–3453. <https://doi.org/10.5194/acp-10-3443-2010>.
- (51) Cooke, C. A.; Balcom, P. H.; Biester, H.; Wolfe, A. P. Over Three Millennia of Mercury Pollution in the Peruvian Andes. *Proc. Natl. Acad. Sci.* **2009**, *106* (22), 8830–8834. <https://doi.org/10.1073/pnas.0900517106>.
- (52) Guerero, S. Chemistry as a Tool for Historical Research: Identifying Paths of Historical Mercury Pollution in the Hispanic New World. *Bull Hist Chem* **2012**, *37*, 61–70.
- (53) Roser, M.; Ritchie, H.; Ortiz-Ospina, E. World Population Growth. Published Online at OurWorldInData.Org. Retrieved from: “<https://Ourworldindata.Org/World-Population-Growth>.” 2013.
- (54) Bagnato, E.; Tamburello, G.; Avard, G.; Martinez-Cruz, M.; Enrico, M.; Fu, X.; Sprovieri, M.; Sonke, J. E. Mercury Fluxes from Volcanic and Geothermal Sources: An Update. *Geol. Soc. Lond. Spec. Publ.* **2015**, *410* (1), 263–285. <https://doi.org/10.1144/SP410.2>.
- (55) Andres, R. J.; Kasgnoc, A. D. A Time-Averaged Inventory of Subaerial Volcanic Sulfur Emissions. *J. Geophys. Res. Atmospheres* **1998**, *103* (D19), 25251–25261. <https://doi.org/10.1029/98JD02091>.
- (56) Carn, S. A.; Fioletov, V. E.; McLinden, C. A.; Li, C.; Krotkov, N. A. A Decade of Global Volcanic SO₂ Emissions Measured from Space. *Sci. Rep.* **2017**, *7* (1), 44095. <https://doi.org/10.1038/srep44095>.
- (57) Kocman, D.; Horvat, M.; Pirrone, N.; Cinnirella, S. Contribution of Contaminated Sites to the Global Mercury Budget. *Environ. Res.* **2013**, *125*, 160–170. <https://doi.org/10.1016/j.envres.2012.12.011>.
- (58) Agnan, Y.; Le Dantec, T.; Moore, C. W.; Edwards, G. C.; Obrist, D. New Constraints on Terrestrial Surface–Atmosphere Fluxes of Gaseous Elemental Mercury Using a Global Database. *Environ. Sci. Technol.* **2016**, *50* (2), 507–524. <https://doi.org/10.1021/acs.est.5b04013>.
- (59) Fitzgerald, W.F. and Lamborg, C.H.,. Geochemistry of Mercury. Treatise on Geochemistry: Volume 9: Environmental Geochemistry; 2004.
- (60) Lamborg, C. H.; Von Damm, K. L.; Fitzgerald, W. F.; Hammerschmidt, C. R.; Zierenberg, R. Mercury and Methylmercury in Fluids from Sea Cliff Submarine Hydrothermal Field, Gorda Ridge. *Geophys. Res. Lett.* **2006**, *33* (17), L17606. <https://doi.org/10.1029/2006GL026321>.
- (61) Bowman, K. L.; Hammerschmidt, C. R.; Lamborg, C. H.; Swarr, G. J.; Agather, A. M. Distribution of Mercury Species across a Zonal Section of the Eastern Tropical South Pacific Ocean (U.S. GEOTRACES GP16). *Mar. Chem.* **2016**, *186*, 156–166. <https://doi.org/10.1016/j.marchem.2016.09.005>.
- (62) Demers, J. D.; Blum, J. D.; Zak, D. R. Mercury Isotopes in a Forested Ecosystem: Implications for Air-Surface Exchange Dynamics and the Global Mercury Cycle. *Glob. Biogeochem. Cycles* **2013**, *27* (1), 222–238. <https://doi.org/10.1002/gbc.20021>.

- (63) Zheng, W.; Obrist, D.; Weis, D.; Bergquist, B. A. Mercury Isotope Compositions across North American Forests: Mercury Isotopes Across U.S. Forests. *Glob. Biogeochem. Cycles* **2016**, *30* (10), 1475–1492. <https://doi.org/10.1002/2015GB005323>.
- (64) Hersbach, H.; Bell, B.; Berrisford, P.; Hirahara, S.; Horányi, A.; Muñoz-Sabater, J.; Nicolas, J.; Peubey, C.; Radu, R.; Schepers, D.; Simmons, A.; Soci, C.; Abdalla, S.; Abellan, X.; Balsamo, G.; Bechtold, P.; Biavati, G.; Bidlot, J.; Bonavita, M.; De Chiara, G.; Dahlgren, P.; Dee, D.; Diamantakis, M.; Dragani, R.; Flemming, J.; Forbes, R.; Fuentes, M.; Geer, A.; Haimberger, L.; Healy, S.; Hogan, R. J.; Hólm, E.; Janisková, M.; Keeley, S.; Laloyaux, P.; Lopez, P.; Lupu, C.; Radnoti, G.; de Rosnay, P.; Rozum, I.; Vamborg, F.; Villaume, S.; Thépaut, J.-N. The ERA5 Global Reanalysis. *Q. J. R. Meteorol. Soc.* **2020**, *146* (730), 1999–2049. <https://doi.org/10.1002/qj.3803>.
- (65) Slemr, F.; Seiler, W.; Schuster, G. Latitudinal Distribution of Mercury over the Atlantic Ocean. *J. Geophys. Res.* **1981**, *86* (C2), 1159. <https://doi.org/10.1029/JC086iC02p01159>.
- (66) Bieser, J.; Slemr, F.; Ambrose, J.; Brenninkmeijer, C.; Brooks, S.; Dastoor, A.; DeSimone, F.; Ebinghaus, R.; Gencarelli, C. N.; Geyer, B.; Gratz, L. E.; Hedgecock, I. M.; Jaffe, D.; Kelley, P.; Lin, C.-J.; Jaegle, L.; Matthias, V.; Ryjkov, A.; Selin, N. E.; Song, S.; Travnikov, O.; Weigelt, A.; Luke, W.; Ren, X.; Zahn, A.; Yang, X.; Zhu, Y.; Pirrone, N. Multi-Model Study of Mercury Dispersion in the Atmosphere: Vertical and Interhemispheric Distribution of Mercury Species. *Atmospheric Chem. Phys.* **2017**, *17* (11), 6925–6955. <https://doi.org/10.5194/acp-17-6925-2017>.
- (67) Sprovieri, F.; Pirrone, N.; Bencardino, M.; D'Amore, F.; Carbone, F.; Cinnirella, S.; Mannarino, V.; Landis, M.; Ebinghaus, R.; Weigelt, A.; Brunke, E.-G.; Labuschagne, C.; Martin, L.; Munthe, J.; Wängberg, I.; Artaxo, P.; Morais, F.; Barbosa, H. de M. J.; Brito, J.; Cairns, W.; Barbante, C.; Diéguez, M. del C.; Garcia, P. E.; Dommergue, A.; Angot, H.; Magand, O.; Skov, H.; Horvat, M.; Kotnik, J.; Read, K. A.; Neves, L. M.; Gawlik, B. M.; Sena, F.; Mashyanov, N.; Obolkin, V.; Wip, D.; Feng, X. B.; Zhang, H.; Fu, X.; Ramachandran, R.; Cossa, D.; Knoery, J.; Maruscak, N.; Nerentorp, M.; Norstrom, C. Atmospheric Mercury Concentrations Observed at Ground-Based Monitoring Sites Globally Distributed in the Framework of the GMOS Network. *Atmospheric Chem. Phys.* **2016**, *16* (18), 11915–11935. <https://doi.org/10.5194/acp-16-11915-2016>.
- (68) Zhang, Y.; Jacob, D. J.; Horowitz, H. M.; Chen, L.; Amos, H. M.; Krabbenhoft, D. P.; Slemr, F.; St. Louis, V. L.; Sunderland, E. M. Observed Decrease in Atmospheric Mercury Explained by Global Decline in Anthropogenic Emissions. *Proc. Natl. Acad. Sci.* **2016**, *113* (3), 526–531. <https://doi.org/10.1073/pnas.1516312113>.
- (69) Strode, S. A.; Jaeglé, L.; Selin, N. E.; Jacob, D. J.; Park, R. J.; Yantosca, R. M.; Mason, R. P.; Slemr, F. Air-Sea Exchange in the Global Mercury Cycle: MERCURY AIR-SEA EXCHANGE. *Glob. Biogeochem. Cycles* **2007**, *21* (1). <https://doi.org/10.1029/2006GB002766>.
- (70) Bieser, J.; Angot, H.; Slemr, F.; Martin, L. *Atmospheric Mercury in the Southern Hemisphere & Part 2: Source Apportionment Analysis at Cape Point Station, South Africa*; preprint; Gases/Field Measurements/Troposphere/Chemistry (chemical composition and reactions), 2020. <https://doi.org/10.5194/acp-2020-63>.

Figures Captions

Figure 1. Profiles of Hg accumulation rates (HgAR) in the peat cores from Amsterdam Island (AMS), Falkland Islands (SCB, Islas Malvinas), Andorra and Harberton (AND, HBT, Tierra del Fuego). Vertical dashed lines operationally separate the natural background (pre-1450AD), pre-industrial (1450-1880AD), the extended 20th century maximum HgAR (20Cmax, grey bars) and modern (post-1990AD) reference periods, following reference ¹⁵).

Figure 2. Review of published Hg accumulation rates (HgAR) and enrichment factors (EF) in NH and SH peat and sediment cores for different reference time periods. HgAR ($\mu\text{g m}^{-2} \text{yr}^{-1}$) and EF in peat (A), (C) and sediment (B), (D) profiles during different periods: Natural background (pre-1450AD), pre-industrial (1450-1880AD), extended 20th century maximum (20Cmax, defined as the broad 20th century HgAR peak, and modern period (post-1990AD). EF_{p/b}: EF from natural background to pre-industrial period. EF_{preind}: EF from pre-industrial to 20Cmax. EF_{alltime}: EF from natural background to 20Cmax.

Figure 3. Hg enrichment factors between different reference time periods and peat background Hg accumulation rate. Enrichment factors (EF) in Hg accumulation rates for A) 20th century industrial relative to pre-industrial periods (EF_{pre-ind}, 1450-1880AD). B) 20th century industrial relative to natural background periods (EF_{alltime}, pre-1450AD century). Circles represent peat cores, and crosses sediment cores. C) Natural background Hg accumulation rate (pre-1450AD HgAR) in peat cores as a function of latitude. For details see Extended Data 2.

Table 1. Hg accumulation rate (HgAR) enrichment factor observed in the peat profiles from this study.

AMS, Amsterdam Island; SCB, the Falkland Islands; AND, HBT, Andorra and Harberton, Argentina. 'Pre-ind', pre-industrial; '20Cmax', extended 20th century maximum HgAR (see Methods); 'p/b', pre-industrial/background.

	Pre-ind/ background (EF _{p/b})	20Cmax/Pre-ind (EF _{preind})	20Cmax/background (EF _{alltime})
AMS	1.6	1.7	2.7
SCB	0.6	2.5	1.5
AND		3.0	
HBT	1.4	5.3	7.3

Table 2. Summary of Hg accumulation rate (HgAR) enrichment factors (EF) in global peat and sediment records. 'Pre-ind', pre-industrial; '20Cmax', extended 20th century maximum HgAR (see Methods); 'p/b', pre-industrial/background; 'modern/back', 'modern/background'; NH, northern hemisphere; SH, southern hemisphere.

	Pre-ind /background (EF _{p/b})		20Cmax/pre-ind (EF _{preind})		20Cmax/background (EF _{alltime})		Modern/ background (EF _{mod/bck})	
Global-sediment	1.6	n=13	2.9	n=103	4.3	n=14	5.0	n=10
Global-peat	2.5	n=17	4.3	n=30	14.5	n=25	10.3	n=18
NH-sediment+peat	3.9	n=18	3.3	n=110	16.1	n=26	10.5	n=17
SH-sediment+peat	1.3	n=11	1.9	n=21	4.0	n=13	3.5	n=11
NH-sediment	3.7	n=5	3.1	n=84	12.8	n=5	19.3	n=4
NH-peat	3.9	n=14	4.6	n=25	16.2	n=21	12.3	n=14
SH-sediment	1.4	n=8	1.8	n=17	3.8	n=97	5.0	n=8
SH-peat	1.2	n=3	3.1	n=4	6.0	n=4	3.1	n=4

¹the number of records, n, do not always add up due to the 2 σ outlier tests applied, for ex. SH sediment, n=8, SH peat, n=3, but SH sediment+peat, n=10. See Methods and Extended Data 2 for details on outlier tests.

Table 3. Summary of natural and anthropogenic Hg emissions to the atmosphere (mean \pm 1 σ)

	NH	1 σ	SH	1 σ
passive volcanic degassing (this study) Mg y ⁻¹	92	20	87	19
eruptive volcanic degassing (this study) Mg y ⁻¹	10	10	10	10
crustal degassing ^{57,58} Mg y ⁻¹	91	27	44	13
anthropogenic 20Cmax emissions ⁷ Mg y ⁻¹	2000	500	480	20
Mean EF _{emission}	11.2	4.6	4.4	1.5
Median EF _{alltime}	16.1	10-30 IQR	4.0	2-6 IQR

Supporting Information

Unequal anthropogenic enrichment of mercury in Earth's Northern and Southern Hemispheres.

Chuxian Li^{1,2}, Jeroen E. Sonke^{2§}, Gaël Le Roux¹, Natalia Piotrowska³, Nathalie Van der Putten⁴, Stephen J. Roberts⁵, Tim Daley⁶, Emma Rice⁶, Roland Gehrels⁷, Maxime Enrico^{1,2,8}, Dmitri Mauquoy⁹, Thomas P. Roland¹⁰, François De Vleeschouwer¹¹

1. Laboratoire écologie fonctionnelle et environnement, Université de Toulouse, CNRS, Toulouse, France

2. Laboratoire Géosciences Environnement Toulouse, Université de Toulouse, CNRS, IRD, UPS, Toulouse, France.

3. Silesian University of Technology, Institute of Physics-CSE, Gliwice, Poland.

4. Faculty of Science, Vrije Universiteit Amsterdam, the Netherlands.

5. British Antarctic Survey, Cambridge, UK

6. School of Geography, Earth and Environmental Sciences, Plymouth University, Plymouth PL4 8AA, UK

7. Department of Environment & Geography, University of York, Heslington, York YO10 5NG, UK

8. Harvard John A. Paulson School of Engineering & Applied Sciences, Harvard University, Cambridge, MA, USA

9. Geography and Environment, School of Geosciences, University of Aberdeen, St Mary's Building, Aberdeen, AB24 3UF, UK

10. Geography, College of Life and Environmental Sciences, University of Exeter, UK

11. Instituto Franco-Argentino para el Estudio delClima y sus Impactos (UMI 3351 IFAECI/CNRS-CONICET-UBA), Universidad de Buenos Aires, Argentina

[§] Corresponding author: jeroen.sonke@get.omp.eu

This SI contains Table S1, S2, Text S1, Figures S1, S2, S3, S4, S5, S6.

Table S1. Details of the coring sites in this investigation

Location	Site name	coordinates	Elevation (m a.s.l)	Precipitation (mm yr ⁻¹)	Coring date	Label core	core length (m)
Amsterdam Island	Central plateau	37.83°S, 77.53°E	738	1124	11/2014	AMS14-PB01	5
Falkland Islands (Islas Malvinas)	San Carlos bog	51.50°S, 58.82°W	8	575	2013	SCB13-PB01C	1.7
Valle de Andorra	Andorra	54.75°S, 68.22°W	198	450-600	02/2012	AND12-PB01W1	0.77
Estancia Harberton	Harberton	54.87°S, 67.22°W	26	600	02/2012	HBT12-PB01W1	0.92

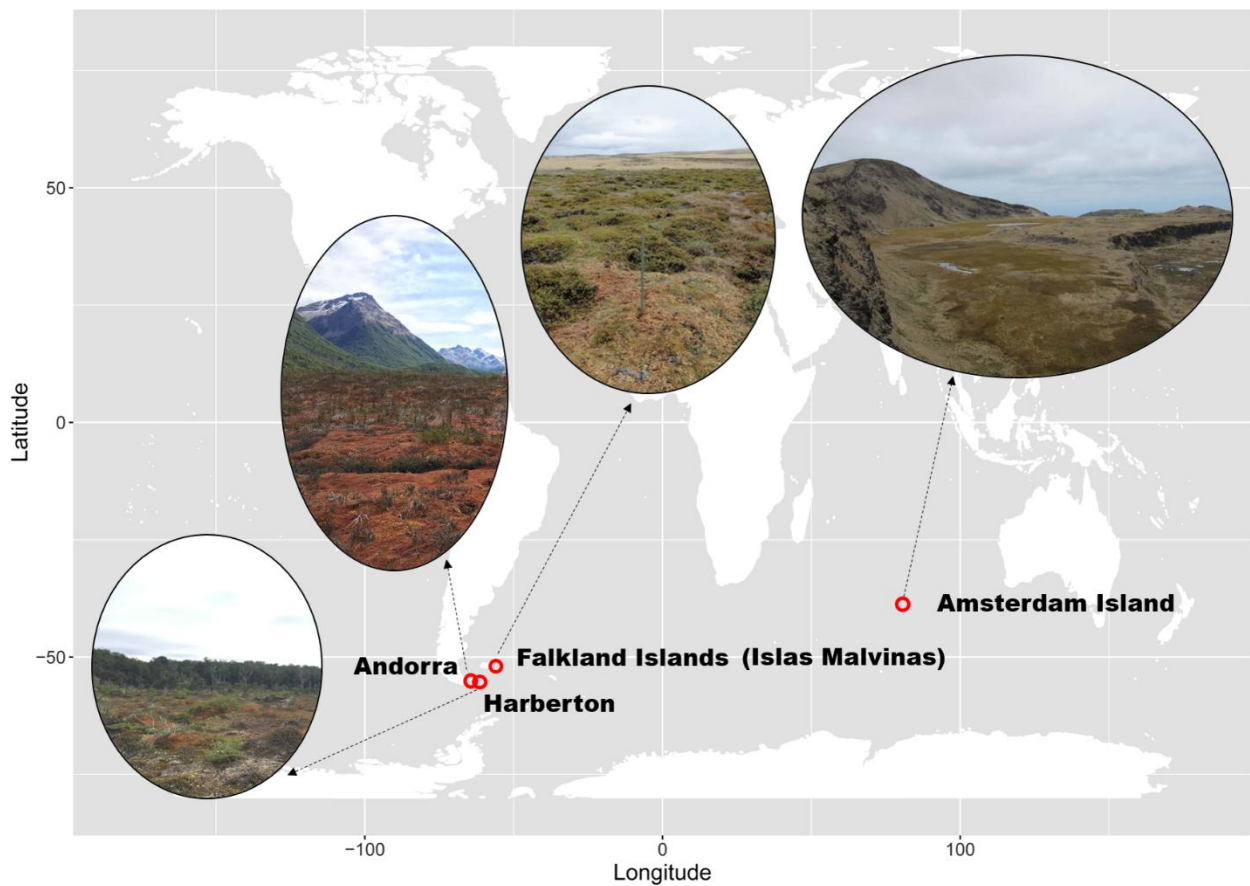


Figure S1. Location of Amsterdam Island (AMS), Falkland Islands (SCB, Islas Malvinas), Andorra (AND) and Harberton (HBT).

Text S1 Core sites:

Amsterdam Island (AMS): A 5 m-long peat sequence (AMS14-PB01A) was collected from the most elevated area of the peatland at 738 m a.s.l. in December 2014 using a stainless steel Russian D-corer of 10 cm internal diameter and 50 cm length. The mean annual temperature at the meteorological station (27 m a.s.l.) is 14°C and annual precipitation is about 1100 mm yr⁻¹ (ref¹). For details about the AMS coring site see ref². The vegetation at the coring site is characterized by bryophytes (brown mosses together with liverworts and some *Sphagnum* species), *Blechnum penna-marina*, *Scirpus aucklandicus*, *Trisetum insularis* and scattered stands of *Agrostis delislei*. Low resolution plant macrofossil data for the last 1000 years from a peat core taken close to the AMS14-PB01A core, with an independent age-depth model, show that the macrofossil record is dominated by higher plant epidermis (c. 70%) until about 400 cal yr BP. For the last 400 years, bryophytes are dominant (70-80%), mainly composed of brown mosses and liverworts, with little occurrence of *Sphagnum* spp. Ash content is <2wt% throughout the core and, together with major element profiles, suggests the site to be ombrotrophic to at least 3.5m depth.

The Falkland Islands (SCB, Islas Malvinas): 'San Carlos bog' is located on the western side of East Falkland Islands (SCB13-PB01C). The native vegetation is treeless and dominated by mosses, grasses and dwarf shrubs^{3,4}. A 1.7 m-long peat sequence was collected from a hummock with an upper monolith section (0 - 50 cm) and lower Russian core section⁵. The surface vegetation of the bog is dominated by *Sphagnum magellanicum*, *Hymenophyllum caespitosum*, *Gaultheria pumila*, *Oreobulis obtusangulus*, *Gunnera magellanica* and *Myrteola nummularia*. The proportion of *Sphagnum* is found to be more than 80% to a depth of 65 cm and followed by herbaceous compacted peat to the bottom. The annual precipitation and temperature are 575 mm yr⁻¹ and 7°C, respectively (data sources from the Falkland Islands Government reported in ref⁴).

Andorra (AND): An ombrotrophic peat monolith (0.72 m length, AND12-PB01W1) was collected at Andorra bog using a stainless steel Wardenaar corer⁶. The AND peat profile is dominated >96% by *Sphagnum magellanicum*. The annual precipitation and temperature are 450-600 mm yr⁻¹ and 6°C, respectively⁷.

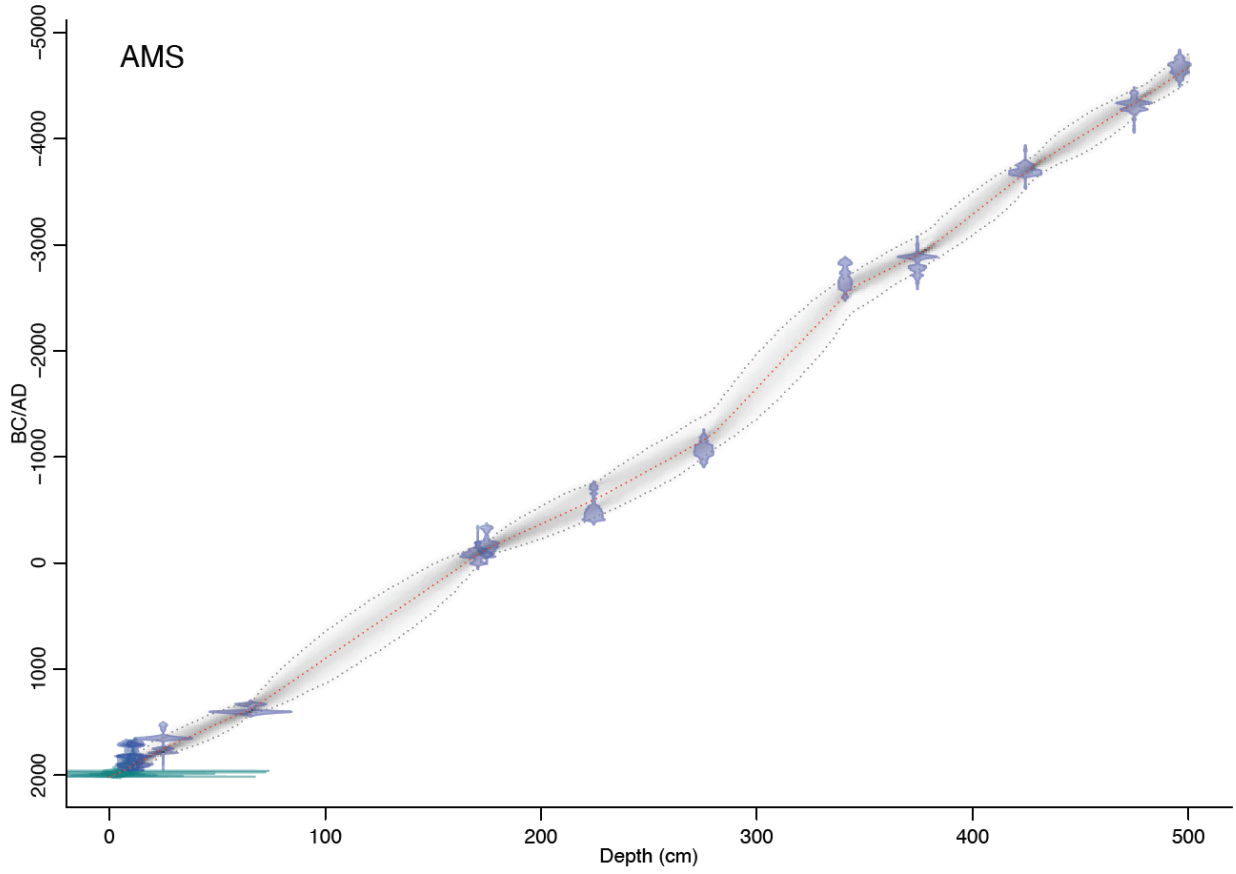
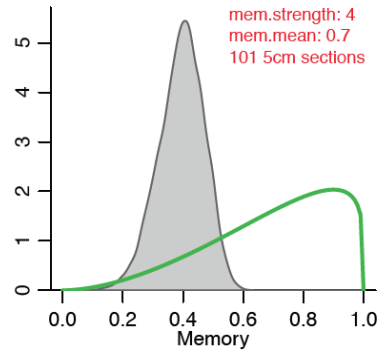
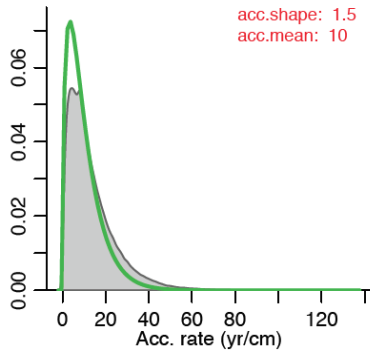
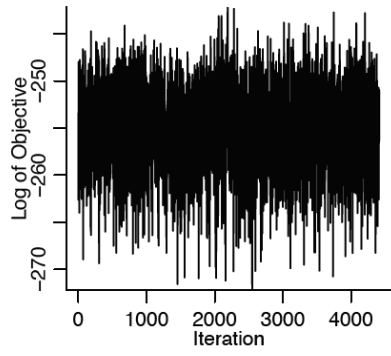
Harberton (HBT): An ombrotrophic peat monolith (0.73 m length, HBT12-PB01W1) was sampled at Harberton Bog by a stainless steel Wardenaar corer⁶. The bog surface is dominated >80% by *Sphagnum magellanicum* with a sparse cover of *Marsippospermum grandiflorum* and *Empetrum rubrum*⁸. The annual precipitation and temperature are around 600 mm yr⁻¹ and 6°C, respectively⁸. We are aware of limited gold mining from 1883 to 1906 on Chilean Islands south of the Beagle Channel, but this is hundreds of kms away from our sites, and late 20th century peaks in HgAR at HBT do not correspond in terms of timing.

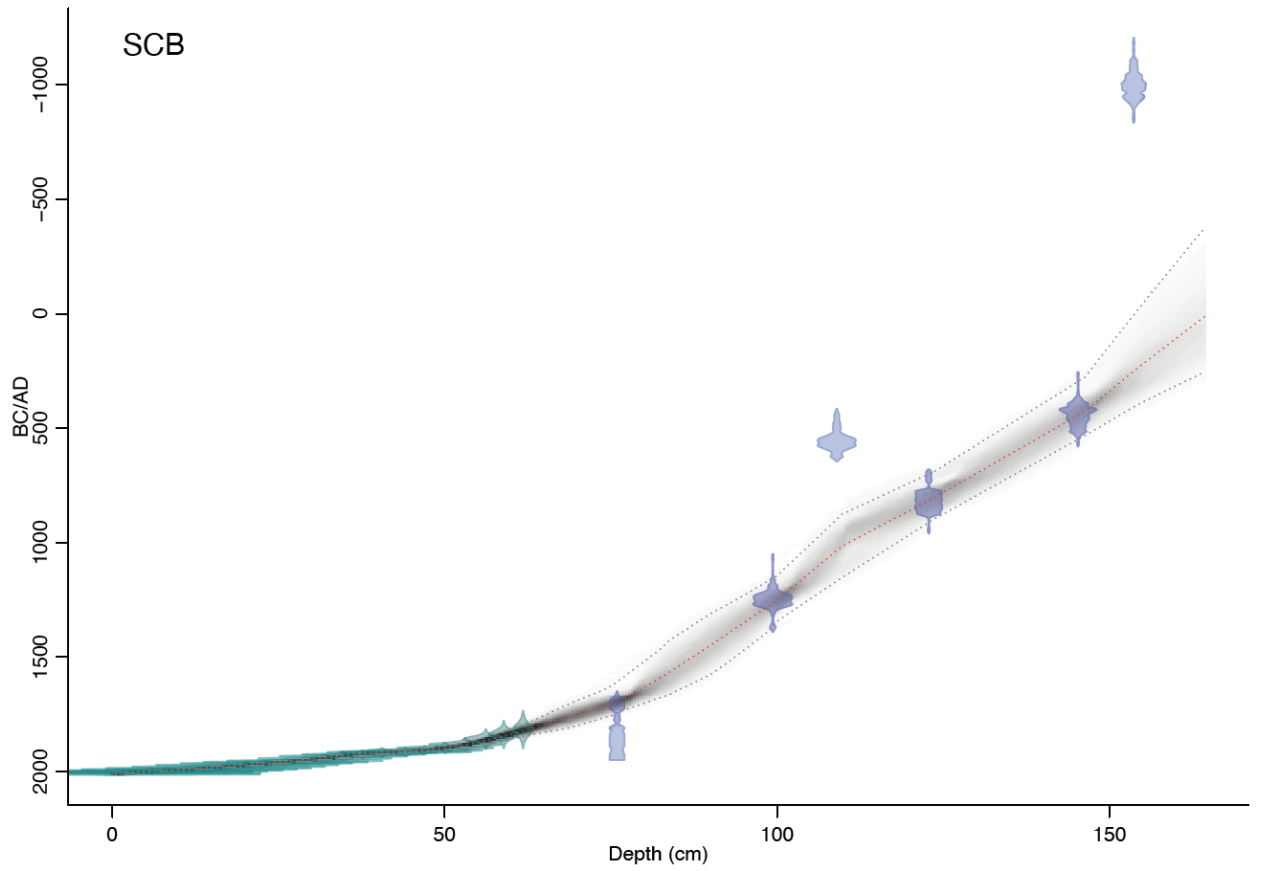
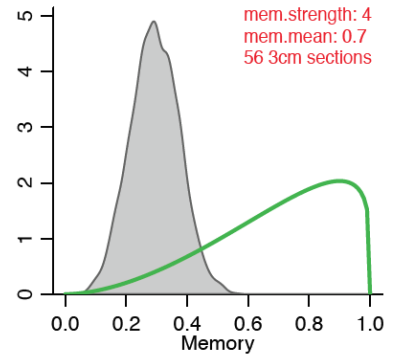
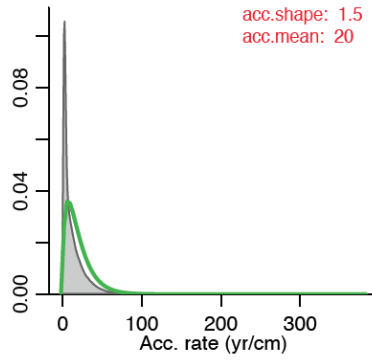
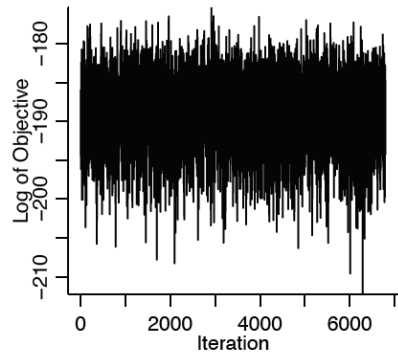
Table S2 Accelerator Mass Spectrometry ¹⁴C dating of plant macrofossils from all the four peat cores.

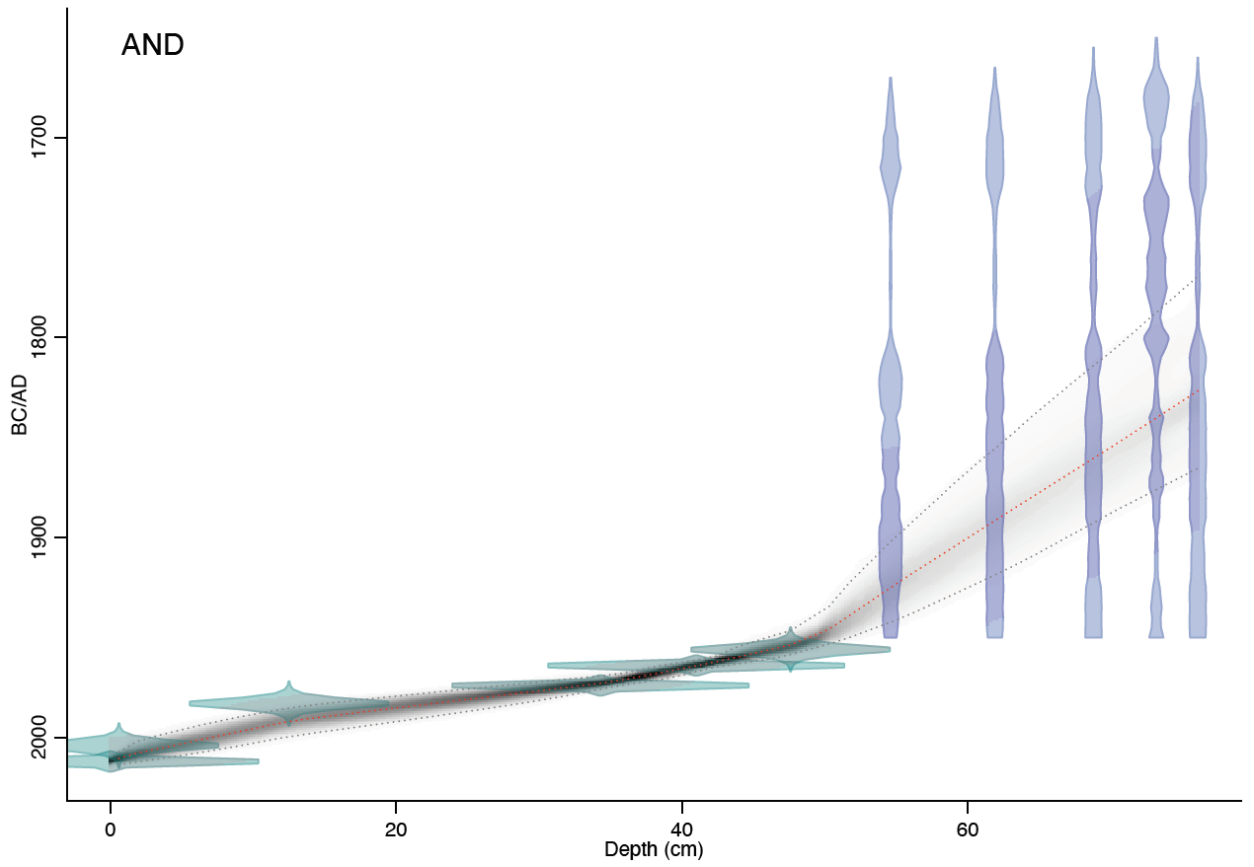
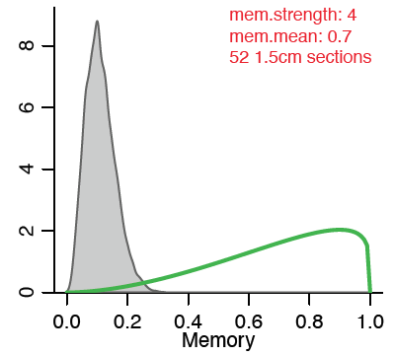
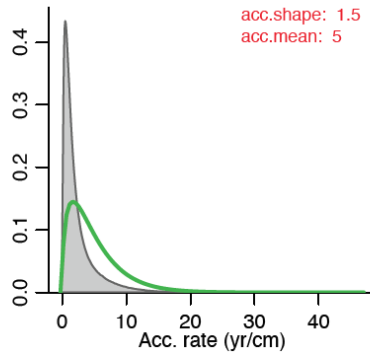
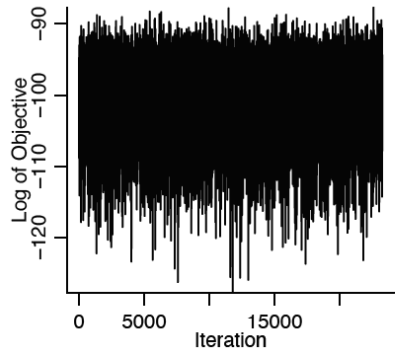
Core name	Lab ID	Mid-Point Depth (cm)	material	Conventional ¹⁴ C Age (yr BP, ± 1σ)	Calibrated age (median, AD/BC)	Modelled age AD/BC (95.4% probability range)
AMS*	SacA50049	2.0	<i>Chorisondontium/Dicranoloma</i> stems + leaves	-557 ± 21	2008 AD	1997-2001 AD
AMS*	SacA50050	3.5	Brown moss stems	-1489 ± 20	1987 AD	1985-1987 AD
AMS*	SacA50051	4.9	Brown moss + liverworts stems	-3052 ± 18	1974 AD	1973-1979 AD
AMS*	SacA50052	6.4	Brown moss + liverworts stems	-1248 ± 20	1960 AD	1956-1962 AD
AMS*	SacA50053	7.8	Brown moss stems	135 ± 30	1942 AD	1938-1950 AD
AMS*	SacA50054	9.4	Brown moss stems	115 ± 30	1928 AD	1917-1937 AD
AMS*	SacA50055	10.8	Brown moss stems + leaves	80 ± 30	1912 AD	1895-1923 AD
AMS*	SacA50056	12.0	Brown moss stems + <i>Chorisondontium/Dicranoloma</i> leaves	160 ± 30	1893 AD	1854-1917 AD
AMS*	SacA50057	13.2	brown moss stems	70 ± 30	1885 AD	1823-1915 AD
AMS*	GdA-4136	24.9	brown moss stems	275 ± 25	1752 AD	1640-1800 AD
AMS*	GdA-4558	65.4	Residue (<i>Sphagnum</i> dominated)	595 ± 25	1389 AD	1310-1440 AD
AMS*	GdA-4560	170.7	Brown moss stems	2100 ± 25	78 BC	155 BC-30 AD
AMS*	GdA-4137	174.8	brown moss stems	2170 ± 30	126 BC	195-55 BC
AMS*	GdA-4138	224.4	brown moss stems	2430 ± 30	580 BC	750-415 BC
AMS*	GdA-4139	275.4	brown moss stems	2925 ± 30	1142 BC	1380-980 BC
AMS*	GdA-4561	340.9	brown moss stems	4145 ± 35	2535 BC	2965-2275 BC
AMS*	GdA-4140	374.4	<i>Sphagnum</i>	4285 ± 30	2900 BC	3075-2750 BC
AMS*	GdA-4141	424.4	<i>Sphagnum</i> + brown moss	4960 ± 30	3680 BC	3795-3550 BC
AMS*	GdA-4142	474.8	<i>Sphagnum</i> stems	5515 ± 35	4330 BC	4460-4190 BC
AMS*	GdA-4143	495.9	<i>Sphagnum</i> stems	5860 ± 35	4615 BC	4750-4470 BC
SCB	SUERC-51676	76.5	<i>Sphagnum</i>	153 ± 37	1694 AD	1597-1737 AD
SCB	GdA-3755	99.9	Undefined peat macrofossils	814 ± 41	1256 AD	1147-1345 AD
SCB	GdA-4744	109.8	Charcoal + Monocyledons undifferentiated (leaf bases)	1553 ± 25	1009 AD	876-1152 AD
SCB	GdA-4745	123.7	Monocyledons undifferentiated (leaf bases)	1261 ± 21	804 AD	688-896 AD
SCB	GdA-4746	146.3	Monocyledons undifferentiated (leaf bases)	1661 ± 25	428 AD	277-532 AD
SCB	GdA-4742	154.3	Charcoal + Monocyledons undifferentiated (leaf bases)	2882 ± 22	252 AD	19 BC-396 AD
SCB	GdA-3756	164.3	Undefined peat macrofossils	11582 ± 50	36 AD	376 BC-254 AD
AND	SacA50058	0.6	<i>Sphagnum</i>	-594 ± 19	2004 AD	2007-2014 AD
AND	SacA50059	13.1	<i>Sphagnum</i>	-1749 ± 19	1983 AD	1985-2000 AD
AND	SacA50060	34.3	<i>Sphagnum</i>	-2839 ± 17	1974 AD	1969-1976 AD
AND	SacA50061	41.0	<i>Sphagnum</i>	-2695 ± 18	1964 AD	1961-1967 AD
AND	SacA50062	47.6	<i>Sphagnum</i>	-67 ± 21	1954 AD	1947-1958 AD
AND	SacA50063	54.6	<i>Sphagnum</i>	120 ± 30	1926 AD	1902-1942 AD
AND	SacA50064	61.9	<i>Sphagnum</i>	140 ± 30	1893 AD	1856-1919 AD
AND	SacA50065	68.8	<i>Sphagnum</i>	160 ± 30	1863 AD	1814-1893 AD
AND	GdA-3032	73.2	<i>Sphagnum</i>	193 ± 23	1843 AD	1787-1876 AD
AND	SacA50066	76.1	<i>Sphagnum</i>	150 ± 30	1831 AD	1769-1865 AD
HBT	SacA42507	0.3	<i>Sphagnum</i>	-424 ± 21	2010 AD	2010-2019 AD
HBT	SacA42508	4.7	<i>Sphagnum</i>	-606 ± 22	2004 AD	2002-2012 AD
HBT	SacA42509	6.9	<i>Sphagnum</i>	-677 ± 21	2002 AD	1999-2008 AD
HBT	SacA42510	9.1	<i>Sphagnum</i>	-788 ± 21	1999 AD	1996-2005 AD
HBT	SacA42511	11.3	<i>Sphagnum</i>	-838 ± 22	1998 AD	1994-2002 AD
HBT	SacA42512	13.6	<i>Sphagnum</i>	-914 ± 21	1996 AD	1991-1999 AD
HBT	SacA44490	15.8	<i>Sphagnum</i>	-1092 ± 22	1992 AD	1988-1996 AD

HBT	SacA44491	19.2	<i>Sphagnum</i>	-1333 ± 21	1988 AD	1984-1992 AD
HBT	SacA44492	21.3	<i>Sphagnum</i>	-1513 ± 20	1985 AD	1981-1989 AD
HBT	SacA44493	26.6	<i>Sphagnum</i>	-2186 ± 21	1979 AD	1974-1982 AD
HBT	SacA44494	31.7	<i>Sphagnum</i>	-2715 ± 20	1975 AD	1964-1976 AD
HBT	SacA44495	37.0	<i>Sphagnum</i>	-2462 ± 27	1964 AD	1930-1964 AD
HBT	SacA44496	43.5	<i>Sphagnum</i>	214 ± 23	1815 AD	1736-1885 AD
HBT	SacA44497	56.2	<i>Sphagnum</i>	407 ± 25	1608 AD	1518-1631 AD
HBT	SacA44498	90.7	<i>Sphagnum</i>	984 ± 24	1148 AD	1063-1216 AD

*Data are from ref²⁸.







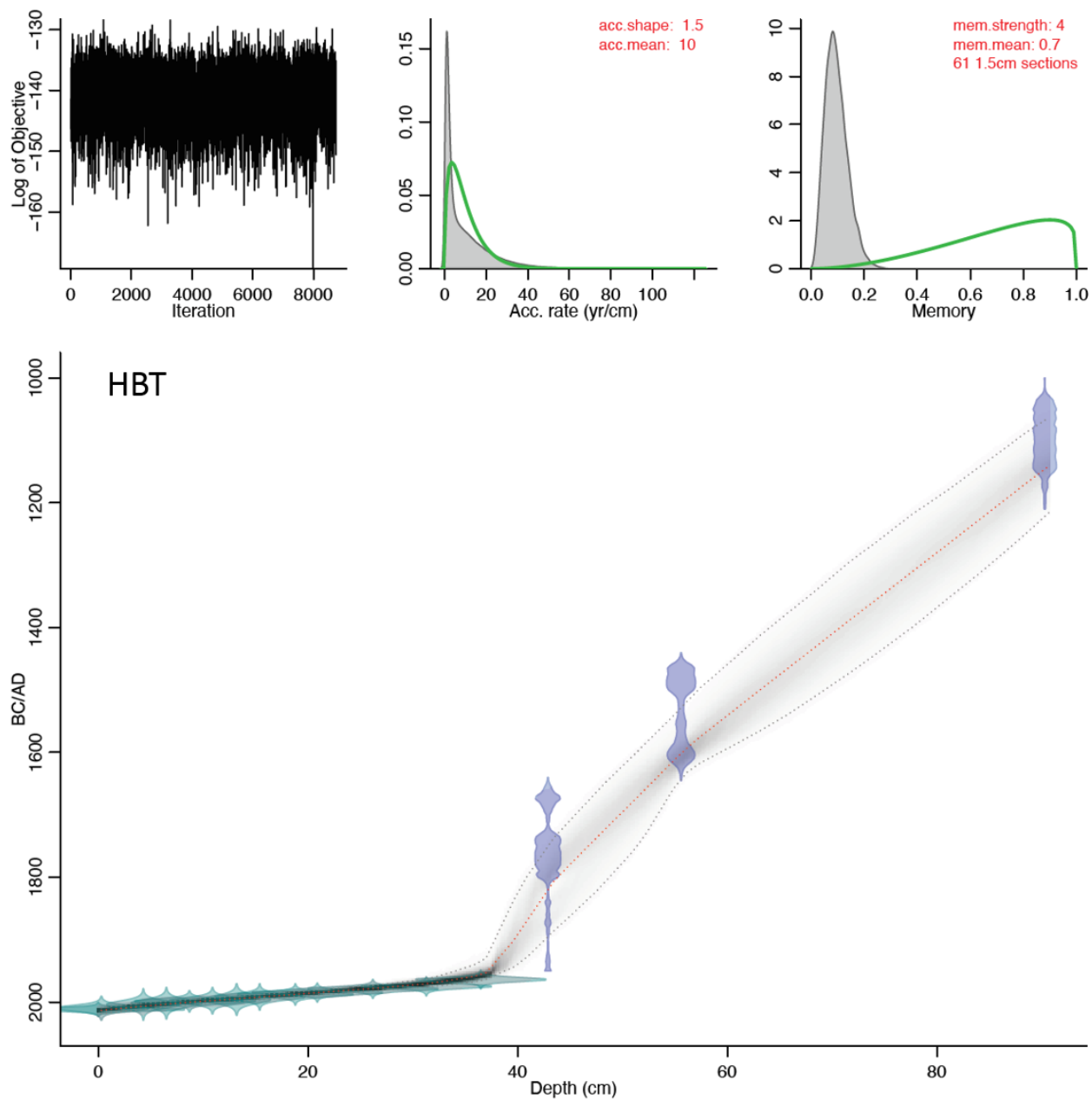


Figure S2. Age models of peat cores from AMS, SCB, AND and HBT using Bacon. Calibrated ^{14}C dates are in transparent blue and ^{210}Pb dates are in transparent green. Red curve indicates single best-fit model based on the weighted mean age for each depth. Darker greys represent more likely calendar ages with 95% confidence intervals shown by grey stippled lines. Diagnostic plots in upper left panels confirm appropriate performance of the models. Settings for accumulation rate and memory are shown in middle and right upper panels (green line—prior, grey shade—posterior distribution), along with thickness and number of sections used for modelling. Prior settings for accumulation rates described by gamma distribution with shape 1.5 and acc.mean 10 or 20 yr/cm, for memory the default beta distribution with parameters mem.strength=4 and mem.mean=0.7 was used.

Table S3 Summary of Hg measurements in standard reference materials.

SRM	materials	Measured value (mean \pm 1 σ , ng g ⁻¹)	Certified value (mean \pm 2 σ , ng g ⁻¹)
IPE 176	Reed/ <i>Phragmites communis</i>	35.1 \pm 6.3 (n=143)	37.9 \pm 2.9
NIST 1632d	Coal	91.3 \pm 7.0 (n=9)	92.8 \pm 3.3
BCR 482	Lichen	481.3 \pm 8.7 (n=5)	480 \pm 20

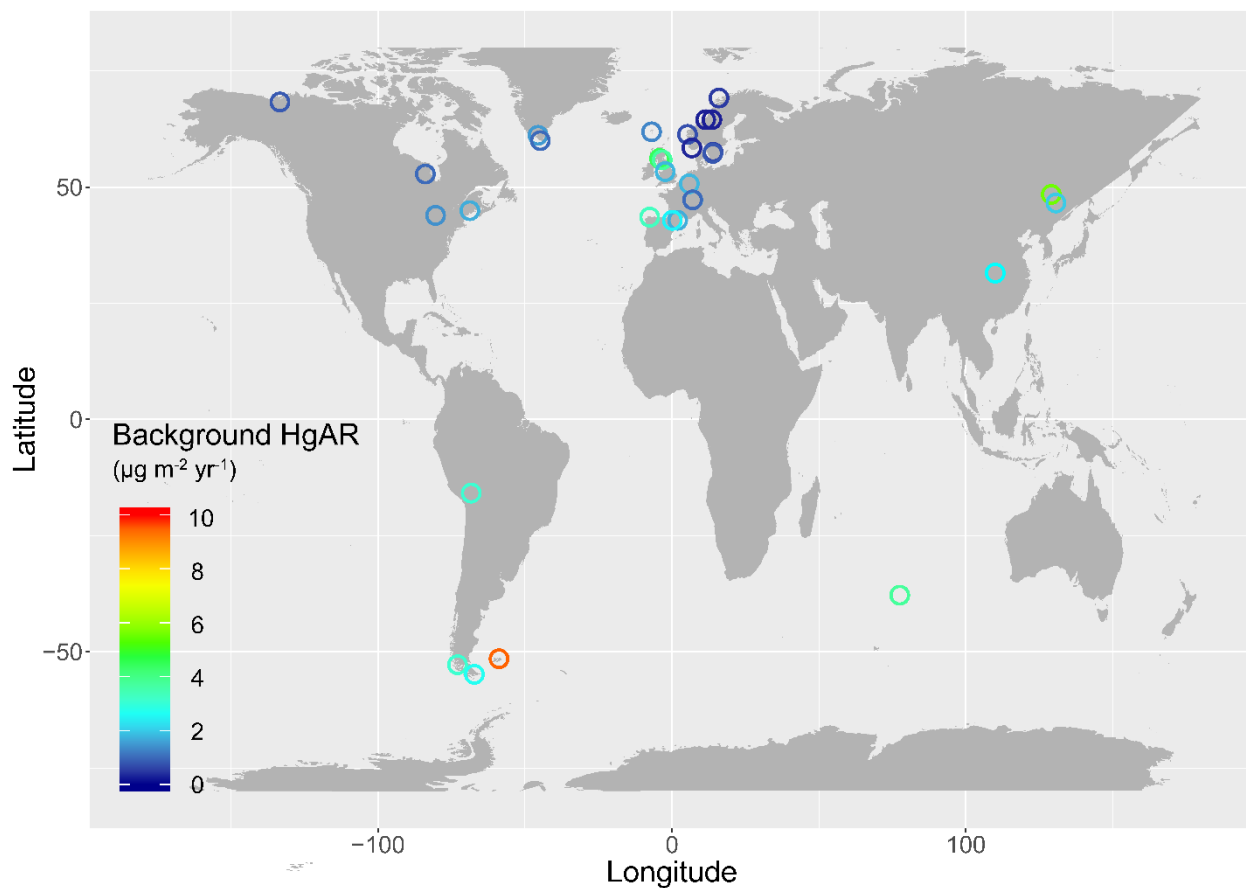


Figure S3. Natural background Hg accumulation rates ($\mu\text{g m}^{-2} \text{yr}^{-1}$) derived from natural peat archives. Details see Extended Data 2.

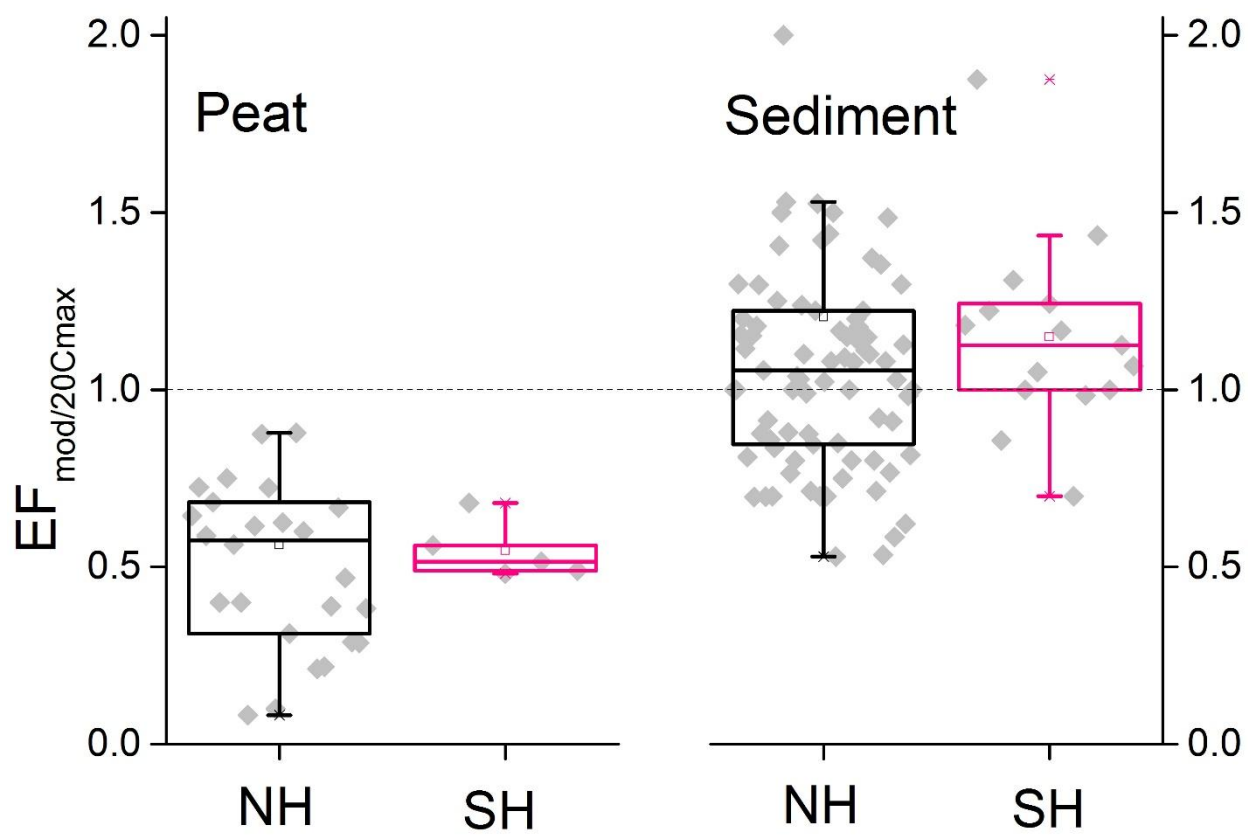


Figure S4. Profiles of HgAR enrichment factor of modern (post-1990) to extended 20th century maximum ($EF_{mod/20Cmax}$) from Northern Hemisphere (NH) and Southern Hemisphere (SH) peat and sediment records. Dashed line indicates $EF=1$.

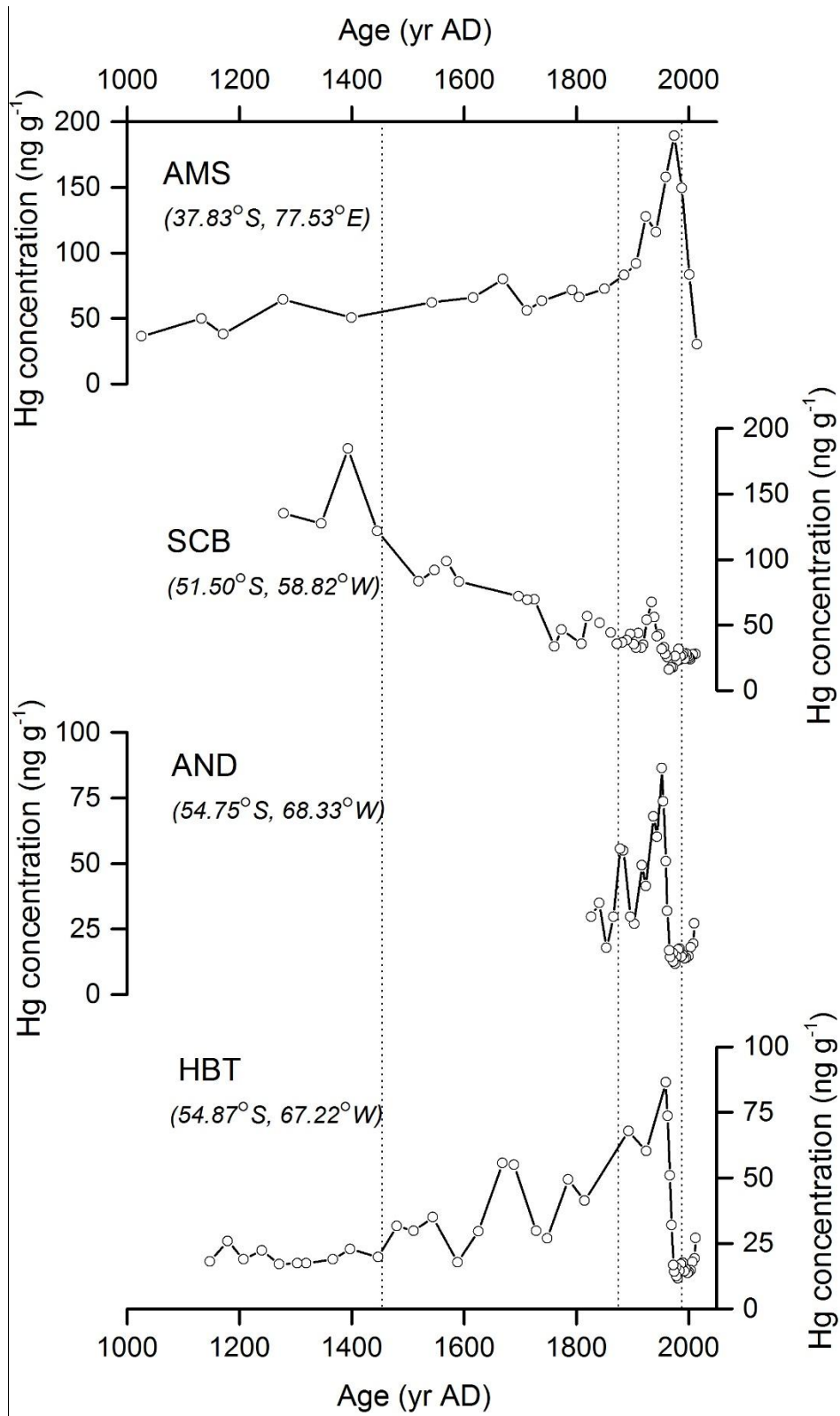


Figure S5. Profiles of Hg concentration (ng g⁻¹) in the peat cores from AMS, SCB, AND and HBT.

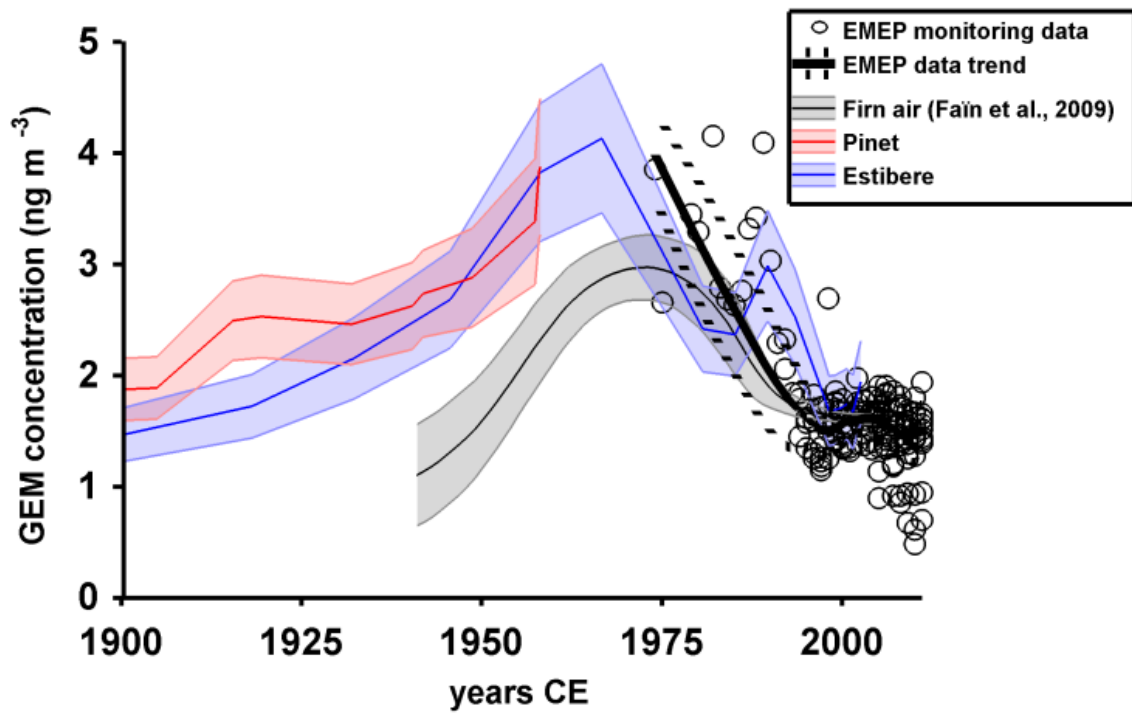


Figure S6. Historical atmospheric Hg monitoring observations and reconstructed Hg levels. Figure reproduced from Enrico et al. 2017, ES&T with permission⁹. Atmospheric gaseous elemental Hg⁰ (GEM) monitoring data (circles) are from EMEP¹⁰.

Supporting Information references

1. Lebouvier, M. and Frenot, Y. Conservation and management in the French sub-Antarctic islands and surrounding seas. In *Papers and proceedings of the royal society of Tasmania*. 207, Vol. 141, No. 1, pp. 23-28.
2. Li, C.; Le Roux, G.; Sonke, J.; van Beek, P.; Souhaut, M.; Van der Putten, N.; De Vleeschouwer, F. Recent ²¹⁰Pb, ¹³⁷Cs and ²⁴¹Am accumulation in an ombrotrophic peatland from Amsterdam Island (Southern Indian Ocean). *Journal of environmental radioactivity*. 2017, 175, pp.164-169.
3. Moore, D.M., 1968. The vascular flora of the Falkland Islands. *The vascular flora of the Falkland Islands.*, (60).
4. Bokhorst, S.; Convey, P.; Huiskes, A.; Aerts, R. Dwarf shrub and grass vegetation resistant to long-term experimental warming while microarthropod abundance declines on the Falkland Islands. *Austral Ecology*. 2017, 42(8), pp.984-994.
5. Belokopytov, I.E. and Beresnevich, V.V. Giktorf's peat borers. *Torfyanaya Promyshlennost*. 1955, 8(9), p.10.
6. Wardenaar, E.C.P. A new hand tool for cutting soil monoliths. *Canadian journal of Soil science*. 1987, 67(2), pp.405-407.
7. Mauquoy, D.; Blaauw, M.; Van Geel, B.; Borronei, A.; Quattrocchio, M.; Chambers, F.M.; Possnert, G. Late Holocene climatic changes in Tierra del Fuego based on multiproxy analyses of peat deposits. *Quaternary Research*. 2004, 61(2), pp.148-158.
8. Vanneste, H., De Vleeschouwer, F.; Martínez-Cortizas, A.; Von Scheffer, C.; Piotrowska, N.; Coronato, A.; Le Roux, G. Late-glacial elevated dust deposition linked to westerly wind shifts in southern South America. *Scientific reports*. 2015, 5, p.11670.
9. Enrico M., et al., Holocene Atmospheric Mercury Levels Reconstructed from Peat Bog Mercury Stable Isotopes. *Environ. Sci. Technol*. 2017, 51, 5899–5906.
10. European Monitoring and Evaluation Programme (2016). <https://www.emep.int/>